

# The effect of biologically mediated decay rates on modelling soil carbon sequestration in agricultural settings

Mohammad Javad Davoudabadi<sup>\*1,2,3,4</sup>, Daniel Pagendam<sup>4</sup>, Christopher Drovandi<sup>1,2,3</sup>, Jeff Baldock<sup>5</sup>, and Gentry White<sup>1,2,3</sup>

<sup>1</sup>*School of Mathematical Sciences, Queensland University of Technology, Australia;*

<sup>2</sup>*Australian Research Council Centre of Excellence for Mathematical & Statistical Frontiers (ACEMS);*

<sup>3</sup>*QUT Centre for Data Science, Queensland University of Technology, Australia;*

<sup>4</sup>*CSIRO Data61, GPO Box 2583, Brisbane, QLD 4001, Australia;*

<sup>5</sup>*CSIRO Agriculture & Food, Glen Osmond, South Australia, Australia;*

## Abstract

Microbial biomass carbon (MBC), a crucial soil labile carbon fraction, is the most active component of the soil organic carbon (SOC) that regulates bio-geochemical processes in terrestrial ecosystems. Some studies in the literature ignore the effect of microbial population growth on carbon decomposition rates. In reality, we might expect that the decomposition rate should be related to the population of microbes in the soil and have a positive relationship with the size of the microbial biomass pool. In this study, we explore the effect of microbial population growth on the accuracy of modelling soil carbon sequestration by developing and comparing two soil carbon models that consider a carrying capacity and limit to the growth of the microbial pool. We apply our models to three datasets, two small and one large datasets, and we select the best model in terms of having the best predictive performance through two model selection methods. Through this analysis we reveal that commonly used complex soil carbon models can over-fit in the presence of both small and large time-series

---

\*mohammadjavad.davoudabadi@hdr.qut.edu.au

datasets, and our simpler model can produce more accurate predictions. We conclude that considering the microbial population growth in a soil carbon model improves the accuracy of a model in the presence of a large dataset.

**Keywords:** Soil carbon sequestration; State-space model ; Rao-Blackwellised particle filter; Correlated pseudo-marginal method; Leave-future-out cross-validation; Model selection.

## 1 Introduction

Modelling soil carbon sequestration plays a crucial role in estimating and forecasting the amount of sequestered carbon in soil and carbon emission from the soil into the atmosphere. This modelling is significant in particular in building decision support systems for land managers selling carbon credits. Selling national carbon credits is in line with the purposes of some international bodies and agreements such as the Intergovernmental Panel on Climate Change (IPCC) and the Paris and Kyoto Protocol agreements to mitigate global warming. Computer-simulation models such as RothC (Jenkinson et al., 1987), FullCAM (Skjemstad et al., 2004), and Century (Parton et al., 1988) have been developed to help make inferences about trends in carbon stocks using time series of measurements collected over many years. The core of these models is made from soil carbon components known as pools. For example, these pools in the RothC model are decomposable plant material (DPM), resistant plant matter (RPM), humified organic matter (HUM), microbial biomass (BIO), and inert organic matter (IOM).

Several studies attempt to quantify uncertainty in soil carbon model outputs through statistical models and sensitivity analysis (running models for different sets of parameter values) (Juston et al., 2010; Paul et al., 2003; Stamati et al., 2013; Yeluripati et al., 2009). Statistical SOC models have some advantages over deterministic SOC models such as RothC, and the main benefit is introducing uncertainties in an SOC model. The uncertainties could be around the parameters, model inputs, dynamics, and subsequently model predictions. Modellers attempt to improve the accuracy of soil carbon models through quantifying uncertainty in model inputs, dynamics, and uncertainties in model parameters within a framework known as Bayesian hierarchical modeling (BHM) (Clifford et al., 2014). Complex models can lead to over-fitting when they are applied to sparse datasets to make inferences about soil carbon stocks. Clifford et al. (2014) address the over-fitting issue by simplifying their model, neglecting some soil organic carbon (SOC) components. Davoudabadi et al. (2021a) apply some advanced Bayesian approaches such as correlated pseudo-

marginal (CPM) method and Rao-Blackwellised particle filters (RBPF) to improve the speed of computation, the accuracy, and the prediction of the model in Clifford et al. (2014).

Microbial biomass carbon (MBC), a crucial soil labile carbon fraction, is the most active component of the SOC that regulates bio-geochemical processes in terrestrial ecosystems (Paul and Clark, 1996). MBC plays a fundamental role in the SOC dynamics and serves as a helpful indicator of changes in soil carbon stabilization and nutrient dynamics following soil management practices (Fierer et al., 2009; Grandy and Neff, 2008; Liang et al., 2011). However, microbial processing of soil organic matter releases  $CO_2$  through respiration which contributes to atmospheric  $CO_2$  and thus global climate change. Some microbially-explicit SOC models are introduced in recent years by considering the effect of the MBC in SOC models (Luo et al., 2016; Blagodatsky et al., 2010; Frey et al., 2013; Moorhead and Sinsabaugh, 2006; Riley et al., 2014; Liu et al., 2020; la Cecilia et al., 2019). Also, several studies consider the complexity of the SOC model and the bio-geochemical realism of models to predict soil carbon stocks (Davoudabadi et al., 2021b; Woolf and Lehmann, 2019). In particular, Davoudabadi et al. (2021b) compared several SOC models by developing a Bayesian model selection method (leave-future-out cross-validation (LFO-CV)) that can identify the soil carbon model with the best predictive performance in light of the available data. Two biologically realistic features are not considered in (Davoudabadi et al., 2021b): (i) decomposition rates that are dependent on the size of the biological (microbe) carbon pool (i.e. more microbes equates to faster rates of decomposition); and (ii) a physical ceiling on the size of the biological (microbial) carbon pool (akin to a carrying capacity in population biology).

Some authors have considered the use of reverse Michaelis-Menten reaction kinetics in modelling soil carbon decomposition as a function of the microbial biomass in the soil (Woolf and Lehmann, 2019; Xie et al., 2020; Wieder et al., 2018). Indeed, reverse Michaelis-Menten reaction kinetics is used to control the microbial decomposition of metabolic and structural litter and available soil organic matter (SOM) pools. Reverse Michaelis-Menten reaction kinetics assumes that the rate of carbon decomposition by the microbe pool, via the action of enzymes, saturates to a maximum rate as the microbial pool grows, see Wieder et al. (2018) for more details. This is a natural way to model the variation in the decomposition rate, with microbe populations consuming the material that they are attached to, but with each particle of substrate only supporting a limited population of microbes, the carrying capacity, and the rate of decomposition, therefore, is limited by this.

In this study, we develop two new SOC models, three and five-pool models. We modify the early version of these models, introduced by (Davoudabadi et al., 2021b) by considering a carrying

capacity or upper limit on the size of the microbial pool and also allowing the size of the microbial pool to moderate the decay rates of the other pools. We call our models BIO-K models. A physical limitation in the size of the microbial biomass pool is intended to reflect that in reality, the microbial biomass pool in soil carbon models is a small proportion. However, the equations that typically govern soil carbon dynamics (e.g., RothC) do not enforce this to be the case.

The framework of our SOC models is the BHM framework used by Davoudabadi et al. (2021b) which is a natural way to account for epistemic uncertainty (uncertainty in the bio-geochemical process dynamics) in a statistically defensible manner. Our focus is on using these models with both the temporally sparse and large datasets. The temporally sparse datasets are two datasets from Tarlee in South Australia and Brigalow in Queensland, Australia (Clifford et al., 2014; Skjemstad et al., 2004), and the large dataset is from the Rothamsted experimental station in Hertfordshire, UK (Rothamsted et al., 1978). These three sites are in different climatic regions. It shows we can apply our approaches to a variety of datasets of any climatic region, and our approaches can be successfully applied to both long-historical and also shorter, sparser datasets. We evaluate our models by two Bayesian model selection methods, leave-future-out cross-validation (LFO-CV) (Bürkner et al., 2020), and widely applicable information criterion (WAIC) (Watanabe and Opper, 2010). LFO-CV is used for small and temporally sparse SOC datasets, while WAIC is more applicable for large datasets. This study is motivated by the question of whether one can gain any benefit in terms of predictive accuracy from considering biologically mediated decay rates in an SOC model. To this end, we compare the predictive accuracy of our BIO-K models with the regular three and five-pool models introduced by Davoudabadi et al. (2021b).

The structure of the paper is as follows. The background and description of datasets are provided in Section 2. Section 3 is devoted to describing the model framework and methods used in this study. We present the structure of our models in Section 4. Sections 5 and 6 present our results and a discussion of this study.

## 2 Background and Description of Datasets

Our model selection method is motivated by three datasets that are collected from three locations in Australia and the UK. The details of these sites are presented in the following.

## 2.1 Tarlee Dataset

Tarlee, situated 80 km north of Adelaide, South Australia, was an agricultural research experiment site established in 1977 to examine the impact of management practices on agricultural productivity as a long term field experiment (Skjemstad and Spouncer, 2003). The classification of the soil of the site is a hard-setting red-brown earth with sandy loam texture. Also, the site is dominated by winter rainfall with an average of 355 mm from April to October and has a Mediterranean climate (Clifford et al., 2014; Luo et al., 2010; Skjemstad et al., 2004). Over a 20-year period, the soil properties of the Tarlee site were monitored in three fields under different management practices. Table 6 in Section B of the supplementary material presents the time period of management treatments that were implemented in three trial fields in Tarlee.

## 2.2 Brigalow Dataset

Brigalow, a research station in Queensland, Australia is situated in a semi-arid, and subtropical climate, and consists of three forested catchments of 12-17 ha (Skjemstad et al., 2004). Within each of the catchments, three monitoring sites were established in recognition of three soil types (a duplex soil and two clays). Wheat and occasional sorghum were planted in one catchment and the other catchment was planted to buffel pasture and the last one was left under native Brigalow forest. At this site, on one catchment, continuous wheat with some sorghum was established over a 18-year period after clearing land under Brigalow (*Acacia harpophylla*) in 1982. Table 7 in Section B of the supplementary material shows the duration of management practices in Brigalow.

## 2.3 Rothamsted Dataset

The Broadbalk continuous wheat experiment is one of the oldest continuous agronomic experiments in the world and was conducted at Rothamsted Research, one of the oldest agricultural research institutions in the world. The Broadbalk study commenced in 1843 and wheat is grown every year on all or part of the experiment. The experiment in section 1 was divided into different plots (labelled 2 - 20) receiving different fertilizer and manure treatments each year. Some treatment plots were established by 1852. Other plots such as 2.1 (2a), 20, and 19 established or became their current size later. Table 8 in Section B of the supplementary material shows the treatments and plots in Broadbalk used in this study.

## 3 Model Framework and Methods

### 3.1 Soil Carbon Model Framework

Three sources of uncertainty in a dynamical SOC model that we consider in this study are errors in the observations, randomness or uncertainty inherent in the underlying physical processes, and uncertainties in model parameters (Clifford et al., 2014). We model these uncertainties through the observation model, the process model, and the prior which are denoted  $p(\mathbf{Y}|\mathbf{X}, \boldsymbol{\theta})$ ,  $p(\mathbf{X}|\boldsymbol{\theta})$ , and  $p(\boldsymbol{\theta})$ , respectively. Here  $\mathbf{Y}$ ,  $\mathbf{X}$ ,  $\boldsymbol{\theta}$ ,  $p(\cdot)$ , and  $p(\cdot|E)$  denote observations, unobserved state process, unknown parameters, the probability density function of the enclosed random variable, and the conditional probability density function given the event  $E$ , respectively. The observation and process models create a model framework known as the state-space model. The state-space model describes a system using indirectly observable variables known as state (or latent) variables and observable measurement variables. Although the state variables cannot be measured directly, one can estimate unobservable state variables based on observable measurement variables that depend on the state variables (Andrieu et al., 2010; Fearnhead and Künsch, 2018). These two hierarchical models typically depend on an unknown parameter vector  $\boldsymbol{\theta}$ . Unknown parameters are treated as random variables in the Bayesian setting and modelled through a parameter model. The model framework created by observation, process, and parameter models is known as Bayesian Hierarchical Model (BHM) that can be represented mathematically as

$$p(\mathbf{Y}, \mathbf{X}, \boldsymbol{\theta}) = p(\mathbf{Y}, \mathbf{X}|\boldsymbol{\theta})p(\boldsymbol{\theta}) = p(\mathbf{Y}|\mathbf{X}, \boldsymbol{\theta})p(\mathbf{X}|\boldsymbol{\theta})p(\boldsymbol{\theta}); \quad (1)$$

where the joint distribution  $p(\mathbf{Y}, \mathbf{X}, \boldsymbol{\theta})$  captures all the uncertainty in the model (Cressie and Wikle, 2015; Berliner, 1996). Through the posterior distribution  $p(\mathbf{X}, \boldsymbol{\theta}|\mathbf{Y})$  we can make inferences about soil carbon dynamics, parameters, and functions of them. This distribution can be written based on (1) as follows

$$p(\mathbf{X}, \boldsymbol{\theta}|\mathbf{Y}) = \frac{p(\mathbf{Y}|\mathbf{X}, \boldsymbol{\theta})p(\mathbf{X}|\boldsymbol{\theta})p(\boldsymbol{\theta})}{p(\mathbf{Y})}; \quad (2)$$

where  $p(\mathbf{Y})$  depends only on data. Evaluating the posterior may be difficult when  $p(\mathbf{Y})$  is analytically intractable. Fortunately, one can make inferences through analytically intractable posterior by drawing samples from it. See (Allenby and Rossi, 2006; Berliner, 1996; Cressie and Wikle, 2015;

Davoudabadi et al., 2021a) for more details about the state-space model and BHM.

As we apply a Bayesian approach for model fitting to quantify the uncertainty in parameters and predictions, we place a prior distribution on the unknown parameter vector  $\boldsymbol{\theta}$  which is shown by  $p(\boldsymbol{\theta})$  in (2). The prior information encompasses three categories; uninformative, weakly informative, and informative. In the case of having a small dataset or sparse dataset over time, the prior distribution becomes more influential, and informative priors can become more useful. We gain prior knowledge in this study from previous studies (Clifford et al., 2014; Davoudabadi et al., 2021b; Skjemstad et al., 2004) and expert opinion. Tables 9, 10, and 11 (Section C) of the supplementary material include the model parameters and their prior probability density functions.

## 3.2 Posterior Distribution Inference

We sample from the posterior distribution  $p(X_{TOC}, \boldsymbol{\theta} | \mathbf{Y})$ , where  $X_{TOC}$  is the mass of total SOC to estimate the changes in SOC over time and to estimate the parameters driving the sequestration of carbon. To do so, as the posterior distribution  $p(\mathbf{X}, \boldsymbol{\theta} | \mathbf{Y})$  in (2) can be decomposed into two components  $p(\mathbf{X} | \boldsymbol{\theta}, \mathbf{Y})p(\boldsymbol{\theta} | \mathbf{Y})$ , we draw samples from that posterior distribution and preserve the components related to the SOC process  $X_{TOC}$  and its parameters  $\boldsymbol{\theta}$ .

As the posterior distribution and the resulting likelihood are not tractable, we apply the correlated pseudo-marginal (CPM) method, one of several particle Markov chain Monte Carlo (PMCMC) methods to the model to draw samples from  $p(\boldsymbol{\theta} | \mathbf{Y})$ . This method improves computational efficiency with respect to other state-of-the-art PMCMC methods by correlating the estimators of the intractable likelihoods in the acceptance ratio of its algorithm. Section D.3 of the supplementary material, Algorithm 3 provides the CPM algorithm. Estimators of the intractable likelihoods are correlated by correlating the auxiliary random numbers used to obtain these estimators, see Deligiannidis et al. (2018); Davoudabadi et al. (2021a,b) for more details. In this algorithm, we generate candidate parameters from appropriate proposal distributions that are presented in the supplementary material Section C. More precisely, proposal distributions are arbitrarily user-specified distributions. If the Markov chain is run for enough iterations, it will converge to the desired posterior distribution. A proper proposal distribution can have a significant influence on the finite-time efficiency of the Markov chain. The ideal case occurs when the proposal distribution is the desired posterior distribution which is typically unknown.

Since the SOC model is a combination of linear and non-linear sub-models, we apply the Rao-

Blackwellised particle filters (RBPF) to draw samples from  $p(\mathbf{X}|\boldsymbol{\theta}, \mathbf{Y})$  and estimate the marginal likelihood of the state variables. The RBPF algorithm estimates the marginal likelihood of the linear and non-linear sub-models through the Kalman Filter (KF) and bootstrap particle filter (BPF), respectively, see Algorithms 1 and 2 in Sections D.1 and D.2 of the supplementary material (Kalman, 1960; Gordon et al., 1993; Doucet et al., 2000; Davoudabadi et al., 2021a). One of the advantages of the RBPF algorithm that makes it an attractive algorithm is that it computes the exact likelihood of the linear sub-model that reduces the computational cost of the estimated likelihood dramatically.

Quantifying uncertainty of our estimate can be done in many ways, for instance, by a 95% credible interval or the estimated expected value of any functions of interest. We can achieve the inference about the mass of SOC added over a period of time by the Markov chain Monte Carlo (MCMC) samples of the posterior distribution. Through MCMC samples  $\{(X^m, \boldsymbol{\theta}^m) : m = 1, \dots, M^*\}$  we represent the posterior distribution  $p(\mathbf{X}, \boldsymbol{\theta}|\mathbf{Y})$  and estimate the posterior expectation of any function  $g^*(\mathbf{X}, \boldsymbol{\theta})$ .

$$\mathbf{E}(g^*(\mathbf{X}, \boldsymbol{\theta})|\mathbf{Y}) \approx \frac{1}{M^*} \sum_{m=1}^{M^*} g^*(X^m, \boldsymbol{\theta}^m). \quad (3)$$

The accuracy of such estimates has a negligible error in the case of having a sufficiently large sample size  $M^*$ . In this study,  $g^*(\mathbf{X}, \boldsymbol{\theta})$  is the change in SOC of the first year of measuring it and following year  $t$ . For instance, in the Tarlee dataset, it is the change in SOC to field  $i$  between 1978 and the following year  $t$

$$g^*(\mathbf{X}, \boldsymbol{\theta}) = X_{TOC(t)}^i - X_{TOC(1978)}^i;$$

which can be estimated through MCMC samples as shown by equation (3).  $X_{TOC(t)}^i$  is the summation of estimated state variables of carbon in all pools at time  $t$  and field  $i$ .

The Gelman and Rubin's convergence diagnostic statistic,  $\hat{R}$ , is a diagnostic check for assessing the quality of the MCMC samples (Gelman and Rubin, 1992). We check the convergence of MCMC samples to the target distribution from multiple PMCMC chains to see whether the output from each chain is indistinguishable, and this occurs when the scale reduction factor is less than 1.2 (Brooks and Gelman, 1998).

The validity of a SOC model to establish its suitability for estimating changes in soil carbon



stocks is vital, in particular, to overcome over-fitting and under-fitting problems when we estimate model parameters and conduct inference with a model. We introduce two methods for model evaluation to select between competing soil carbon models in the next section.

### 3.3 Model Evaluation

Measuring predictive accuracy is a way to validate or compare models (Gelman et al., 2014). In this study, we use two approaches, leave-future-out cross-validation (LFO-CV) (Bürkner et al., 2020) and widely applicable information criterion (WAIC) (Watanabe and Opper, 2010), which are fully Bayesian metrics in the sense that they use the entire posterior distribution. Davoudabadi et al. (2021b) use the LFO-CV to compare the model’s predictive accuracy for four SOC models to understand whether more complex multi-pool models offer the best predictive tool when the datasets available for inference are relatively sparse. We use the same approach for sparse datasets in this paper. To this end, we use the expected log pointwise predictive density (ELPD) as a global measure of predictive accuracy, which is

$$\text{ELPD} = \log \prod_{t=L}^{T-1} \mathbf{E}_{\theta|Y_{1:t}}(p(\tilde{Y}_{t+1}|Y_{1:t}, \theta)) = \sum_{t=L}^{T-1} \log \int p(\tilde{Y}_{t+1}|Y_{1:t}, \theta)p(\theta|Y_{1:t}) d\theta; \quad (4)$$

where  $Y_{1:T} = \{Y_1, \dots, Y_T\}$  is a time series of observations,  $L$  is the minimum number of observations from the series that we will require before making predictions for future data (Bürkner et al., 2020). The parameter space of  $\theta$  in (4) includes state variables as our model is a state-space model, and we should estimate unknown state variables, see Section D.4 of the supplementary material for more details. Typically, the integral in (4) is not analytically tractable, however we can estimate it through Monte-Carlo methods. This can be done by sampling  $(\theta_{1:t}^1, \dots, \theta_{1:t}^S)$  from the posterior distribution  $p(\theta|Y_{1:t})$  for  $t \in \{1, \dots, \gamma\}$  where  $\gamma \in \{L, \dots, T-1\}$  using the particle PMCMC method described in Section 3.2 and estimate the predictive density for  $\tilde{Y}_{L+1:T}$  as follows

$$p(\tilde{Y}_{t+1}|Y_{1:t}) \approx \frac{1}{S} \sum_{s=1}^S p(\tilde{Y}_{t+1}|Y_{1:t}, \theta_{1:t}^s). \quad (5)$$

Although the LFO-CV computes the exact ELPD (hence, exact LFO-CV), it is computationally expensive when used with a larger dataset since it requires re-running the PMCMC to process each data point in time.

The WAIC method is faster than the LFO-CV method as it requires to run the PMCMC once

for all data to get the posterior distribution which makes the WAIC be suitable for larger datasets. We use the WAIC method to explore the predictive accuracy of the soil carbon dynamics models and compare the applied models to a large dataset. The WAIC value by itself is not interpretable. It could be higher than a million, close to zero, or even negative value. When comparing models fitted to the same dataset, the model with the smallest WAIC value is considered to provide the best fit to the data among the candidate models. Gelman et al. (2014) suggest two different ways to measure the effective number of parameters in the WAIC formula which has a general format as follows

$$WAIC = -2 \sum_{t=1}^T \log \int p(Y_t|\boldsymbol{\theta})p(\boldsymbol{\theta}|\mathbf{Y})d\boldsymbol{\theta} + 2\rho_{WAIC}. \quad (6)$$

The first component of (6) is the computed log pointwise posterior predictive density, a measure of fit, and the second component is a correction for the effective number of parameters to adjust for over-fitting. As the first component of (6) is intractable, one can estimate it using  $S$  samples from the posterior

$$\sum_{t=1}^T \log \int p(Y_t|\boldsymbol{\theta})p(\boldsymbol{\theta}|\mathbf{Y})d\boldsymbol{\theta} \approx \sum_{t=1}^T \log \left( \frac{1}{S} \sum_{s=1}^S p(Y_t|\boldsymbol{\theta}^s) \right). \quad (7)$$

Gelman et al. (2014) recommend using  $\sum_{t=1}^T Var_{post}(\log p(Y_t|\boldsymbol{\theta}))$ , the posterior variance of the log predictive density, to estimate the effective number of parameters as it gives results closer to the leave-one-out cross validation (LOO-CV). The WAIC method is asymptotically equivalence with the LOO-CV as the first three terms of the Taylor expansion of WAIC match the Taylor expansion of LOO-CV and Watanabe and Opper (2010) argue that, asymptotically, the latter terms have negligible contribution. We can estimate the posterior variance of the log predictive density in practice by  $\sum_{t=1}^T (\frac{1}{S-1} \sum_{s=1}^S (\log p(Y_t|\boldsymbol{\theta}^s) - \overline{\log p(Y_t|\boldsymbol{\theta}^*)})^2)$ , where  $\overline{\log p(Y_t|\boldsymbol{\theta}^*)}$  is the mean log probability of data point  $Y_t$  across all  $S$  parameter samples. WAIC implicitly assumes that the observations are independent of each other which can be problematic with our state-space model structure as there is usually temporal dependencies in the data. A solution to overcome this is to write  $\log p(Y_t|\boldsymbol{\theta}^s)$  in terms of conditional distributions  $\log p(Y_1|\boldsymbol{\theta}^s) + \sum_{t=2}^T \log p(Y_t|Y_{1:t-1}, \boldsymbol{\theta}^s)$  (Auger-Méthé et al., 2020).

As mentioned earlier, we would like to compare the performance of two SOC models in terms of gaining the best predictive tool based on aforementioned methods. The structure of the models

are introduced in the next section.

## 4 Model Structure

In this study, we introduce two new SOC models that are the modified version of the three-pool and five-pool (RothC-like) models in Davoudabadi et al. (2021b). We investigate how the SOC components and complexity of the SOC models affect the SOC prediction in the presence of large and small time-series datasets. The modified three-pool model consists of three conceptual pools IOM, BIO, and the main pool of decomposable carbon (an amalgamation of DPM, RPM, and HUM pools). Soil carbon decomposes from the decomposable carbon pool, and fractions are either lost to the atmosphere as  $CO_2$  or transferred to the BIO pool. Carbon present in the BIO pool that decomposes is either transferred to the main soil carbon pool, lost to the atmosphere as  $CO_2$ , or re-assimilated as biological mass. The IOM fraction is constant since it is not subject to biological transformation. As such, the IOM process model at time  $t$  is an unknown fixed value and should be estimated. The general carbon emission in the three-pool model can also be represented graphically as depicted in Figure 1a. The process and observation models of the three-pool model are presented in detail in Sections E.1 and E.2 of the supplementary material, respectively.

The general structure of the five-pool model in this study is similar to the RothC-like model introduced in Davoudabadi et al. (2021b). The difference is that we distribute the extra amount of carbon in the BIO pool among other pools in our model. Davoudabadi et al. (2021b) discard the surplus amount of carbon in the BIO pool in their model. Indeed, decomposition of carbon from RPM and DPM pools either leaves the system as  $CO_2$  into the atmosphere or is transformed to carbon in the HUM and BIO pools. Carbon from the HUM and BIO pools that decomposes can either be transformed to carbon in the HUM or BIO pools or lost to the atmosphere as  $CO_2$ . Figure 1b shows the diagram of the carbon emission in the five-pool model. The mathematical representations of the process and observation models of the five-pool model are shown in detail in Sections F.1 and F.2 of the supplementary material, respectively.

### 4.1 Biologically Mediated Decay Rates

Davoudabadi et al. (2021b) consider a constraint in their SOC pools whereby the BIO pool can be at most 5% of the total SOC. This constraint prevents too much carbon from entering the

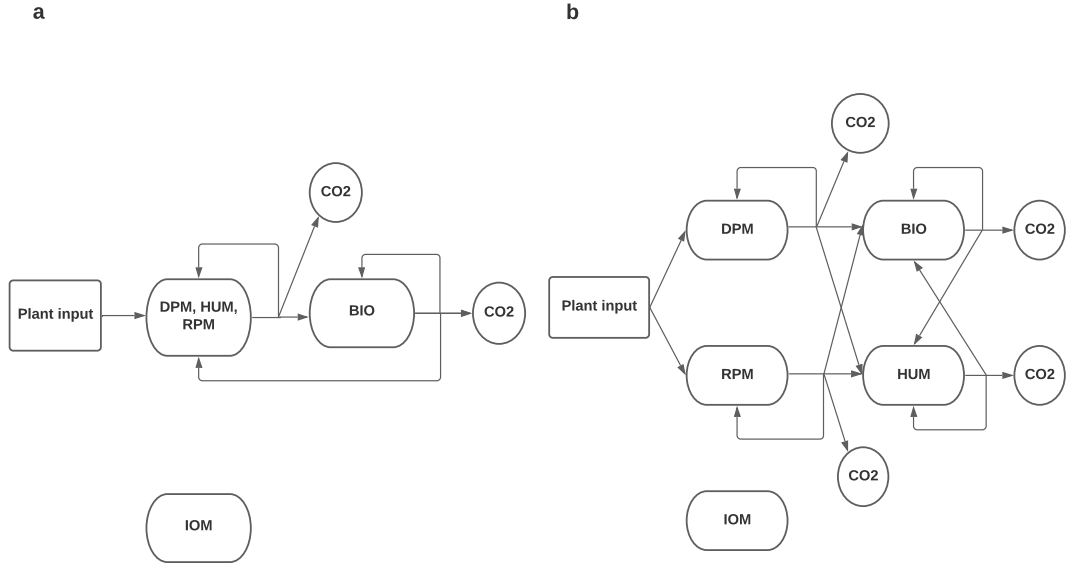


Figure 1: Graphical representation of the carbon emission in the a) three-pool BIO-K model and b) five-pool BIO-K model. The DPM, HUM and RPM pools are amalgamated and treated as a single homogeneous pool in the three-pool model.

microbial pool and where excess, the extra amount is rejected by rejecting BIO state trajectories in the MCMC algorithm. In reality, we might expect that the decomposition rate should be related to the population of microbes in the soil. In other words, we might expect the rates of carbon decomposition to have a positive relationship with the size of the BIO pool. In this study, we include the BIO-pool mediated decay rate in our SOC models using a logistic function with a carrying capacity, and we call our new models, in general, BIO-K models. We impose the dependency of the decomposition rate of carbon pool  $p$  by

$$D_{p(t-1)} = K_p \frac{X_{B(t-1)}}{X_{TOC(t-1)} \kappa_{BIO}}.$$

Where  $D_{p(t-1)}$  is the decomposition rate of pool  $p$  at time  $t - 1$ ,  $K_p$  is the decay rate of pool  $p$ ,  $X_{B(t-1)}$  is the stock of the BIO pool at time  $t - 1$ ,  $X_{TOC(t-1)}$  is the total decomposable soil carbon stock at time  $t - 1$ , and  $\kappa_{BIO} = 0.05$  is the microbial carrying capacity as a percentage of the total decomposable soil carbon. In the three-pool BIO-K model,  $p$  is shown by  $C$  and  $B$  in the amalgamate pool (first pool) and the BIO pool, respectively, and  $K_p$  is shown by  $K_C$  and  $K_B$  as the decay rates of the first and BIO pools, respectively. Also, in the five-pool BIO-K model,  $p$  is denoted by  $R$ ,  $H$ , and  $B$  in pools RPM, HUM, and BIO, respectively and the associated decay

rates of these pools are shown by  $K_R$ ,  $K_H$ , and  $K_B$ , respectively.

In the three-pool BIO-K model, the extra amount of carbon in the microbial pool moves to the first pool, while in the five-pool BIO-K model this extra amount is distributed among other pools. We considered the extra amount in our models based on  $U_{(t-1)}^i - \min(U_{(t-1)}^i, \kappa_{BIO} X_{Total(t-1)}^i - X_{B(t-1)}^i)$ , where  $U_{(t-1)}^i$  is defined for the three and five-pool BIO-K models separately in Sections E.1 and F.1 of the supplementary material, respectively.

## 5 Results

### 5.1 Comparing Models

We fit the three and five pool BIO-K models to the Brigalow and Tarlee datasets, evaluating them through the LFO-CV method as these datasets are small and temporally sparse. To do so, we worked with three PMCMC chains in the CPM method for estimating the predictive density (5). In both the three and five pool BIO-K models, we initialised each chain with a randomly sampled parameter vector and ran them for 200,000 iterations discarding the first 100,000 as burn-in in the Tarlee dataset and 400,000 iterations discarding the first 200,000 as burn-in in the Brigalow dataset. Since we thinned these chains, choosing every 20<sup>th</sup> sample of the MCMC samples to estimate (5),  $S$  in equation (5) for the Tarlee and Brigalow datasets are 5,000 and 10,000, respectively. The minimum numbers of observations,  $L$ , used for making predictions for future data were 12 and 13 in the Tarlee and Brigalow datasets, respectively. Table 1 shows the estimated ELPD of the three and five-pool BIO-K models applied to the Tarlee and Brigalow datasets.

Dataset	Three-pool BIO-K model		Five-pool BIO-K model	
	Mean (ELPD)	SD	Mean (ELPD)	SD
Tarlee	<b>-35.7016</b>	1.4229	-39.0255	1.8519
Brigalow	<b>-40.1425</b>	1.2804	-45.9984	5.2612

Table 1: The mean and standard deviation (SD) of the three chains of the ELPD of the three and five-pool BIO-K models applied to the Tarlee and Brigalow datasets.

Based on these results provided in Table 1, the three-pool BIO-K model outperformed the five-pool BIO-K model in the sense of gaining the best LFO predictive ability for both the Brigalow and Tarlee datasets. Table 2 shows the estimated ELPD of the regular (i.e. without the additional

Dataset	Three-pool model		Five-pool model	
	Mean (ELPD)	SD	Mean (ELPD)	SD
Tarlee	<b>-34.6796</b>	1.9754	-37.2585	1.4591
Brigalow	<b>-36.2252</b>	1.7778	-51.1718	4.6777

Table 2: The mean and standard deviation (SD) of the three chains of the ELPD of the three and five-pool regular models applied to the Tarlee and Brigalow datasets.

dynamics from the BIO-K model) three and five-pool models in Davoudabadi et al. (2021b) applied on the Tarlee and Brigalow datasets. The models in Davoudabadi et al. (2021b) have better predictive accuracy, except the five-pool model of the Brigalow dataset, than the BIO-K models in the presence of temporally sparse datasets. In addition to that, Tables 1 and 2 support the notion that the three-pool model has the better predictive accuracy over the five-pool model that has been frequently used for modeling soil carbon sequestration.

Figures 2 and 3 show the performance of the three and five-pool BIO-K models (columns a and b, respectively) in estimating the trajectories of the SOC dynamics of Brigalow and Tarlee datasets, respectively. As shown in Figures 2b and 3b, the five-pool BIO-K model increased uncertainty in the soil carbon dynamics of both datasets, especially during the sparse periods which is typified by wide 95% credible intervals.

We compared the three and five-pool BIO-K models applied on the Broadbalk dataset based on the WAIC since the dataset is large. Although the SOC measurements in the Broadbalk site is sparse over time, to compare the performance of the models on large datasets, we chose plots 2b, 3, 5, 7, 10, and 14 as they have the most SOC measurements among other plots in the Broadbalk dataset. To compute the WAIC criterion, we worked with three PMCMC chains, each initialised with a randomly sampled parameter vector, for estimating (6). We ran each chain for 100,000 and 150,000 iterations discarding the first 20,000 and 75,000 as burn-in in the three and five-pool BIO-K models, respectively. We ran each chain for 100,000 and 200,000 iterations discarding the first 20,000 and 75,000 as burn-in for the three and five-pool regular models. Tables 3 and 4 show the estimated WAIC of the three and five-pool BIO-K models and regular models, respectively, applied to the Broadbalk dataset.

Based on the results shown in Tables 3 and 4, the three-pool BIO-K model outperforms the five-pool BIO-K and the three-pool regular models in the sense of having lower WAIC value.

Figures 4 and 5 show the performance of the three and five-pool BIO-K models in estimating the trajectories of the SOC dynamics of the Broadbalk dataset, respectively. The performance of

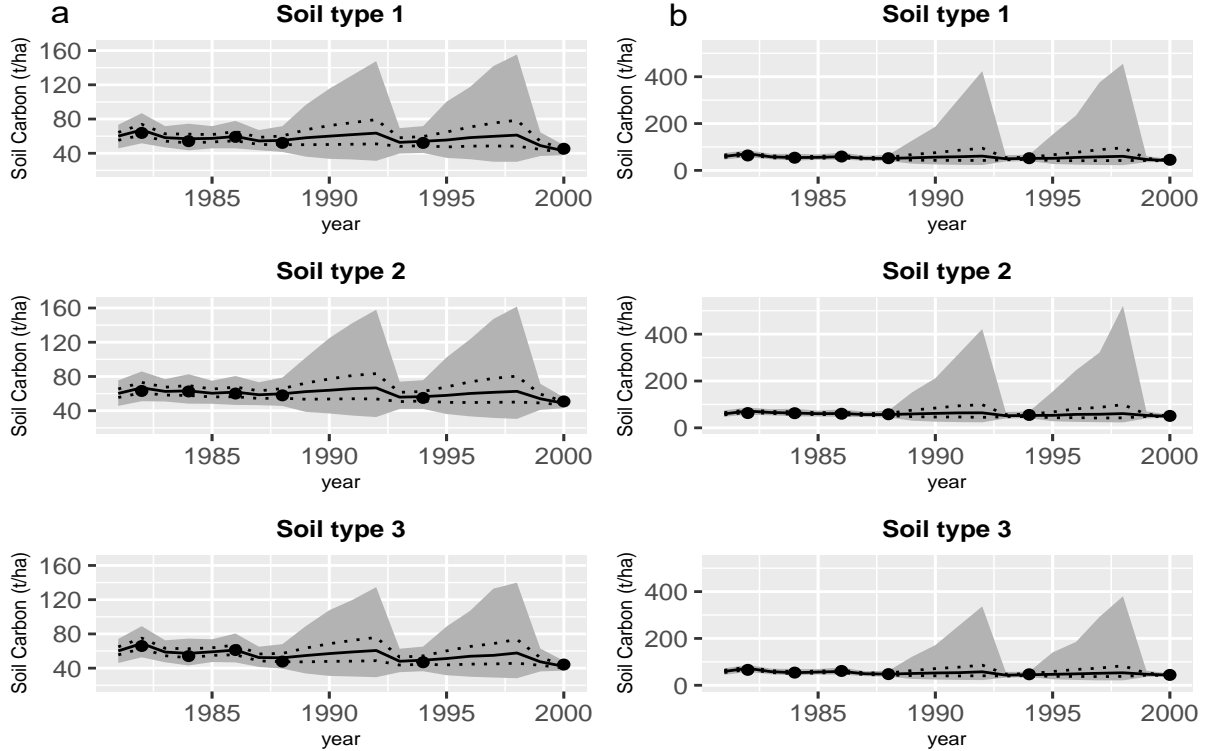


Figure 2: Soil organic carbon (SOC) dynamics of the Brigalow dataset based on a) the three-pool BIO-K model and b) the five-pool BIO-K model. The gray shaded part is the area between the 2.5<sup>th</sup> and the 97.5<sup>th</sup> percentiles for the SOC process gained by the three and five-pool BIO-K models. The 25<sup>th</sup> and the 75<sup>th</sup> percentiles for the SOC process are indicated by the dashed lines. The 50<sup>th</sup> percentile is shown by the solid line and the measured SOC values are indicated by filled dots.

MCMC Chain	Three-pool BIO-K model WAIC	Five-pool BIO-K model WAIC
Chain 1	$173 \times 10^3$	$261 \times 10^3$
Chain 2	$175 \times 10^3$	$252 \times 10^3$
Chain 3	$176 \times 10^3$	$245 \times 10^3$

Table 3: The WAIC of the three MCMC chains of the three and five-pool BIO-K models applied on the Broadbalk dataset.

the three and five-pool regular models in estimating the trajectories of the SOC dynamics of the Broadbalk dataset are shown in Figures 6 and 7, respectively. Note that the 95% credible intervals are related to the trajectories of the process model while the filled dots are the observations of the latent process that have been corrupted by measurement noise.

## 5.2 Uncertainty quantification

Based on the three-pool BIO-K model, the average of the change in equation (3) between years 1978 and 1997 in fields  $\{1, 2, 3\}$  in Tarlee are 1.86, 2.63, and 14.72, respectively. The change of SOC in the Brigalow trial between 1981 and 2000 base on the three-pool BIO-K model are  $-0.45$ ,  $2.93$ , and

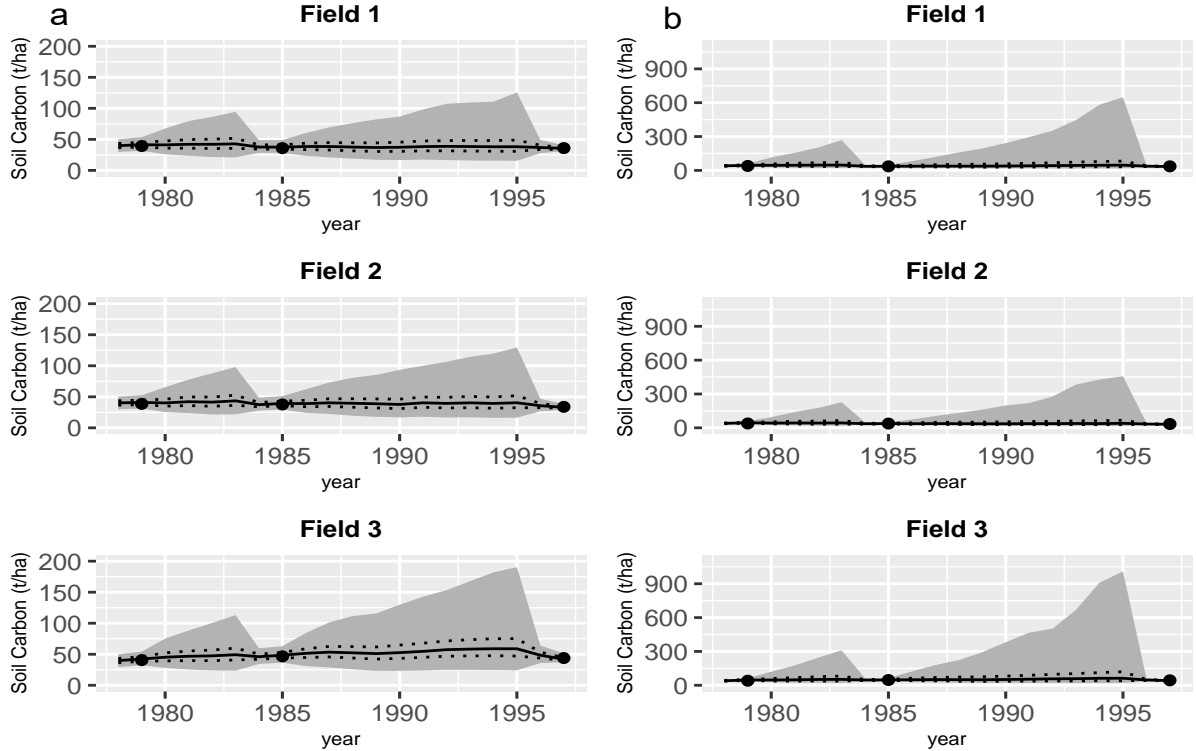


Figure 3: Soil organic carbon (SOC) dynamics of the Tarlee dataset based on a) the three-pool BIO-K model and b) the five-pool BIO-K model. The gray shaded part is the area between the 2.5<sup>th</sup> and the 97.5<sup>th</sup> percentiles for the SOC process gained by the three and five-pool BIO-K models. The 25<sup>th</sup> and the 75<sup>th</sup> percentiles for the SOC process are indicated by the dashed lines. The 50<sup>th</sup> percentile is shown by the solid line and the measured SOC values are indicated by filled dots.

MCMC Chain	Three-pool regular model WAIC	Five-pool regular model WAIC
Chain 1	<b><math>733 \times 10^3</math></b>	$1448 \times 10^3$
Chain 2	<b><math>732 \times 10^3</math></b>	$1533 \times 10^3$
Chain 3	<b><math>736 \times 10^3</math></b>	$1466 \times 10^3$

Table 4: The WAIC of the three MCMC chains of the three and five-pool regular models applied on the Broadbalk dataset.

-2.70, respectively. The average of the change of SOC in plots  $\{2b, 3, 5, 7, 10, 14\}$  of the Broadbalk between years 1852 and 2015 are 76.24, 15.63, 16.68, 19.35, 17.89, and 18.37, respectively.

As mentioned earlier in Section 3.1, prior knowledge of unknown parameters plays a significant role in the presence of small and sparse datasets in a Bayesian setting. We compared a histogram of the samples drawn from the posteriors with the prior distributions of some main model parameters of the three and five-pool BIO-K models to highlight what we have learned about those parameters. Figures 8a and 8b show the difference between the posterior and prior of the decomposition rate of the SOC and BIO pools of the three-pool BIO-K model in Tarlee and Brigalow, respectively. The difference between the posterior and prior of these parameters of the three-pool BIO-K and regular models of the Broadbalk dataset are shown in Figures 9a and 9b, respectively. We presented the



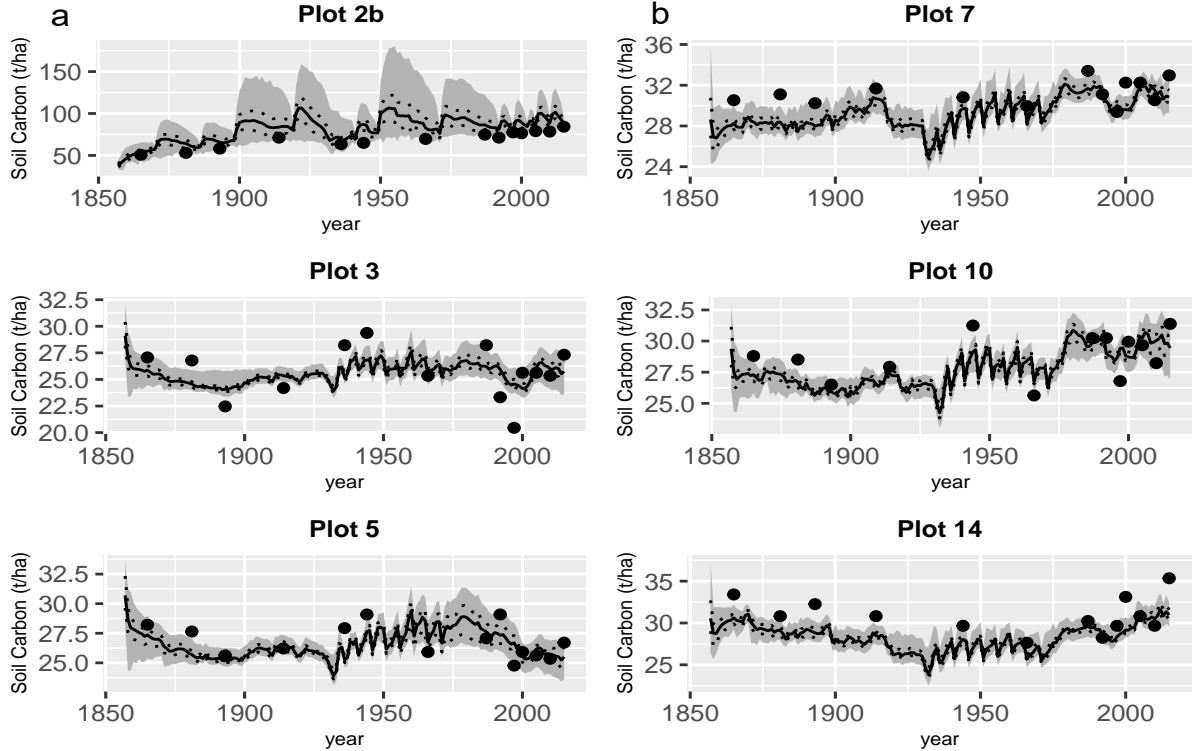


Figure 4: The trajectories of the process model of the soil organic carbon (SOC) dynamics of the Broadbalk dataset based on the three-pool BIO-K model. The gray shaded part is the area between the 2.5<sup>th</sup> and the 97.5<sup>th</sup> percentiles for the SOC process gained by the three-pool BIO-K model. The 25<sup>th</sup> and the 75<sup>th</sup> percentiles for the SOC process are indicated by the dashed lines. The 50<sup>th</sup> percentile is shown by the solid line and the measured SOC values are indicated by filled dots.

difference between the posterior and prior of the decomposition rates in the five-pool BIO-K model of Tarlee and Brigalow in Figures 10a and 10b, respectively.

We computed the Gelman and Rubin’s convergence diagnostics,  $\hat{R}$  for the model parameters of the three-pool BIO-K model of the Tarlee, Brigalow, and Broadbalk datasets which are presented in Tables 12, 13, and 14, respectively, in Section G of the supplementary material. The Gelman and Rubin’s convergence diagnostics,  $\hat{R}$  for the model parameters of the three-pool Regular model of the Broadbalk dataset are presented in Table 15 in Section G of the supplementary material.

## 6 Discussion

In this study, we have developed two SOC models to explore the impact of microbial population growth on estimating the amount of sequestered carbon in farmlands. We have also compared the predictive ability of the three-pool model with the more complex and frequently used five-pool (RothC-like) model. We have implemented these models on three datasets, two of them are small and sparse over time, and the other one is large, to show they are broadly applicable.

Microbial population growth has a positive relationship with carbon decomposition rate and

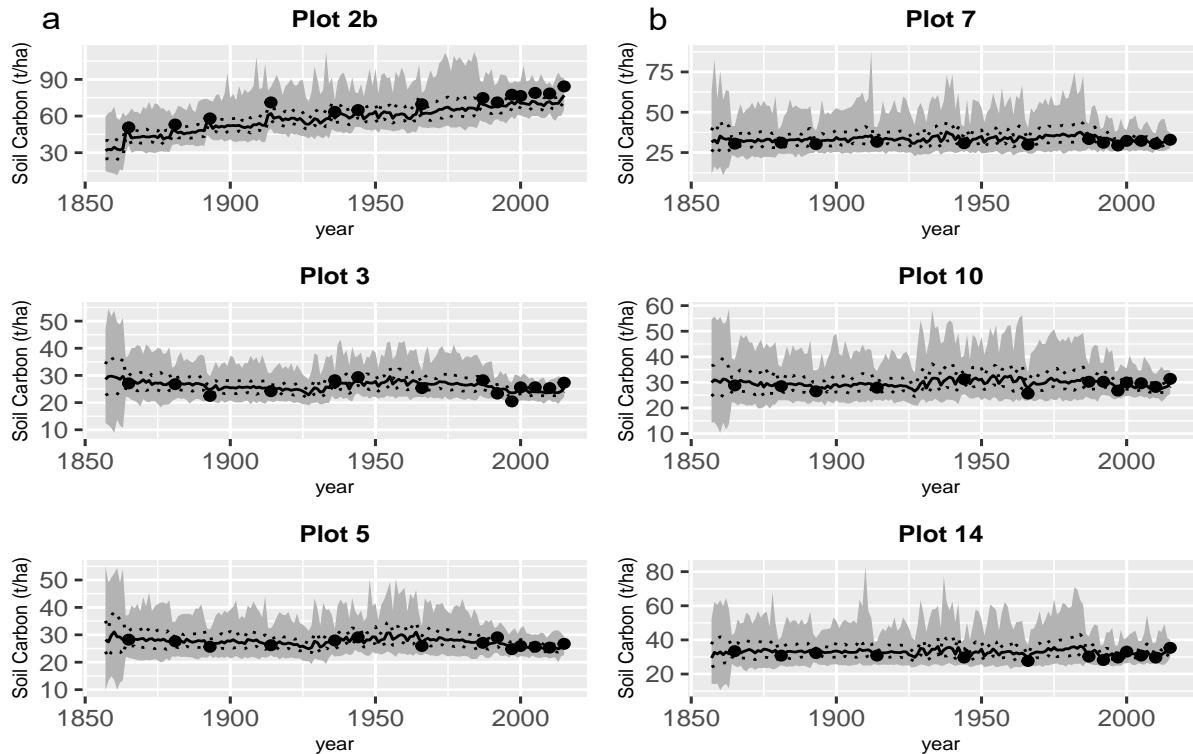


Figure 5: The trajectories of the process model of the soil organic carbon (SOC) dynamics of the Broadbalk dataset based on the five-pool BIO-K model. The gray shaded part is the area between the 2.5<sup>th</sup> and the 97.5<sup>th</sup> percentiles for the SOC process gained by the five-pool BIO-K model. The 25<sup>th</sup> and the 75<sup>th</sup> percentiles for the SOC process are indicated by the dashed lines. The 50<sup>th</sup> percentile is shown by the solid line and the measured SOC values are indicated by filled dots.

has a dynamic process. The motivating question behind this study is whether considering the decay rates of soil carbon pools as being mediated by the size of the microbial pool in SOC models can improve the accuracy of the SOC models for making inferences on soil carbon dynamics. We fitted the three and five-pool BIO-K models on three datasets, and we found that a three-pool BIO-K model (in all datasets) to have a better predictive ability than the five-pool BIO-K model. Also, we compared the predictive abilities of the three and five-pool BIO-K models with the regular three and five-pool models in Davoudabadi et al. (2021b) through fitting them on the Tarlee, Brigalow, and Broadbalk datasets. Based on their LFO-CV and WAIC values, the three-pool model introduced by Davoudabadi et al. (2021b) outperforms the three-pool BIO-K model in both Tarlee and Brigalow but the three-pool BIO-K model has a better predictive ability than the regular three-pool model in the presence of a large dataset, the Broadbalk dataset. Although considering the microbial population growth did not improve the accuracy of the SOC models when making inferences on soil carbon dynamics of small datasets, we showed that the three-pool model outperforms the five-pool model in both regular and BIO-K models. It supports the idea that some concessions in physical realism can lead to better predictive accuracy that can be helpful

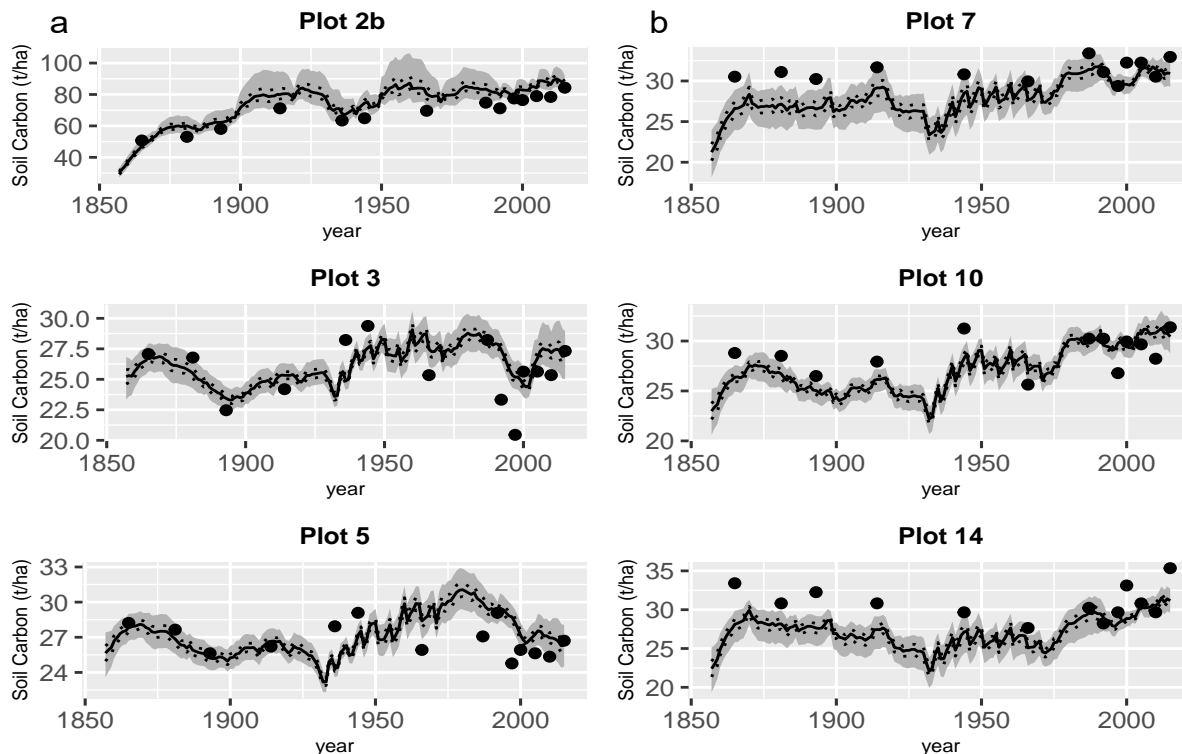


Figure 6: The trajectories of the process model of the soil organic carbon (SOC) dynamics of the Broadbalk dataset based on the three-pool regular model. The gray shaded part is the area between the 2.5<sup>th</sup> and the 97.5<sup>th</sup> percentiles for the SOC process gained by the three-pool regular model. The 25<sup>th</sup> and the 75<sup>th</sup> percentiles for the SOC process are indicated by the dashed lines. The 50<sup>th</sup> percentile is shown by the solid line and the measured SOC values are indicated by filled dots.

for national carbon accounting.

We have successfully shown that a frequently used multi-pool model, the RothC model, might not be as fit-for-purpose compared to the three-pool model when used with both temporally sparse and large datasets. Davoudabadi et al. (2021b) show that a farmer or a land manager can gain more accuracy in making inferences about soil carbon sequestration when the three-pool model is applied to small datasets. Our study suggests that a three-pool model may not only be suitable for modelling short, short sparse datasets (see Davoudabadi et al. (2021b)) but also for much longer historical datasets.

One of the advantages of our models and the models introduced in Davoudabadi et al. (2021b) is that the SOC dynamics are modelled on a yearly time step that makes these models easier to fit and analyse (statistically) compared to models that consider the SOC changes on a monthly time step. Our main argument for embracing the yearly time-step arises from the fact that crop yields are often reported on an annual basis. For models that operate on a monthly time-step, annual yield data must then be dis-aggregated using some sort of model to try and determine how much carbon entered the soil for each month. Not only is this dis-aggregation a difficult undertaking,

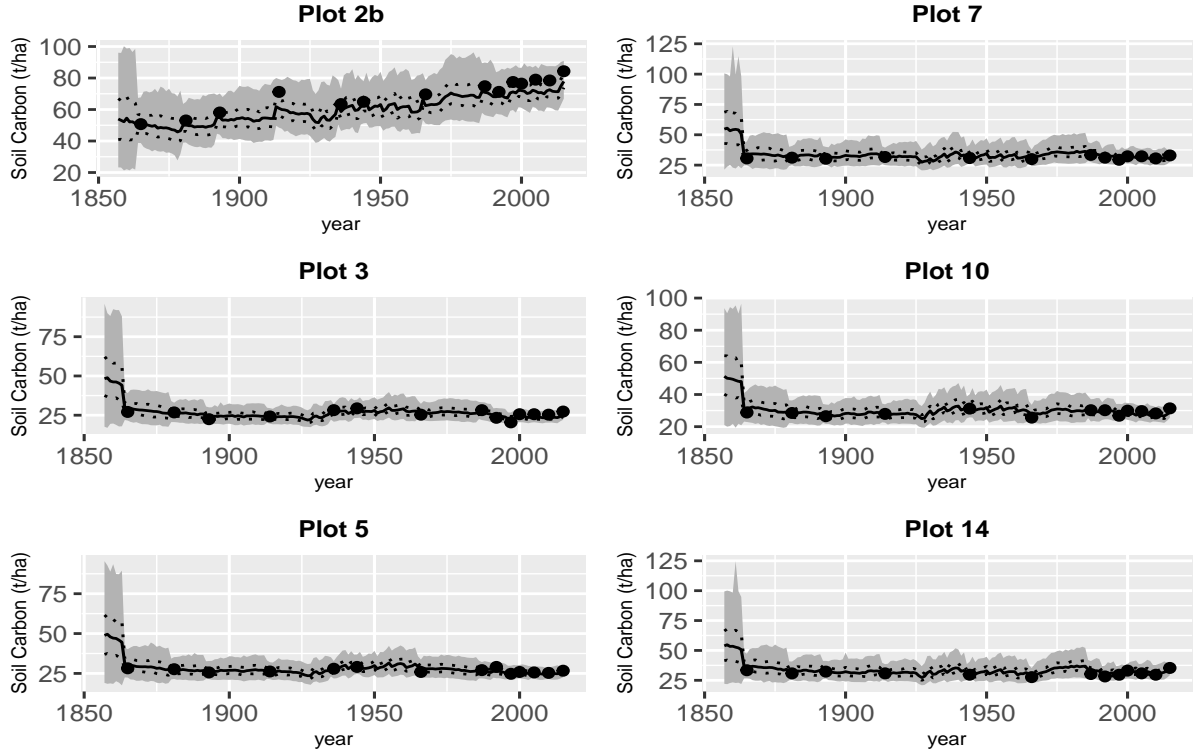


Figure 7: The trajectories of the process model of the soil organic carbon (SOC) dynamics of the Broadbalk dataset based on the five-pool regular model. The gray shaded part is the area between the 2.5<sup>th</sup> and the 97.5<sup>th</sup> percentiles for the SOC process gained by the five-pool regular model. The 25<sup>th</sup> and the 75<sup>th</sup> percentiles for the SOC process are indicated by the dashed lines. The 50<sup>th</sup> percentile is shown by the solid line and the measured SOC values are indicated by filled dots.

but it is a major source of uncertainty in the modelling since these soil carbon inputs are a major driver of the soil carbon dynamics.

Many long-term datasets are available that our models and methods have not been tested over those datasets to estimate the global  $CO_2$  emission from soil. We will consider this in the future study.

## 7 Acknowledgments

We would like to thank CSIRO for providing the Tarlee and Brigalow datasets used in this study. MJD was supported by QUT-CSIRO Digital Agriculture Scholarship and a CSIRO Digital Agriculture Top-Up Scholarship. CD was supported by the Australian Research Council. We gratefully acknowledge the computational resources provided by QUT's High Performance Computing (HPC) and Research Support Group. We thank the Lawes Agricultural Trust and Rothamsted Research for data from the e-RA database. The Rothamsted Long-term Experiments National Capability (LTE-NC) is supported by the UK BBSRC (Biotechnology and Biological Sciences Research Council, BBS/E/C/000J0300) and the Lawes Agricultural Trust.

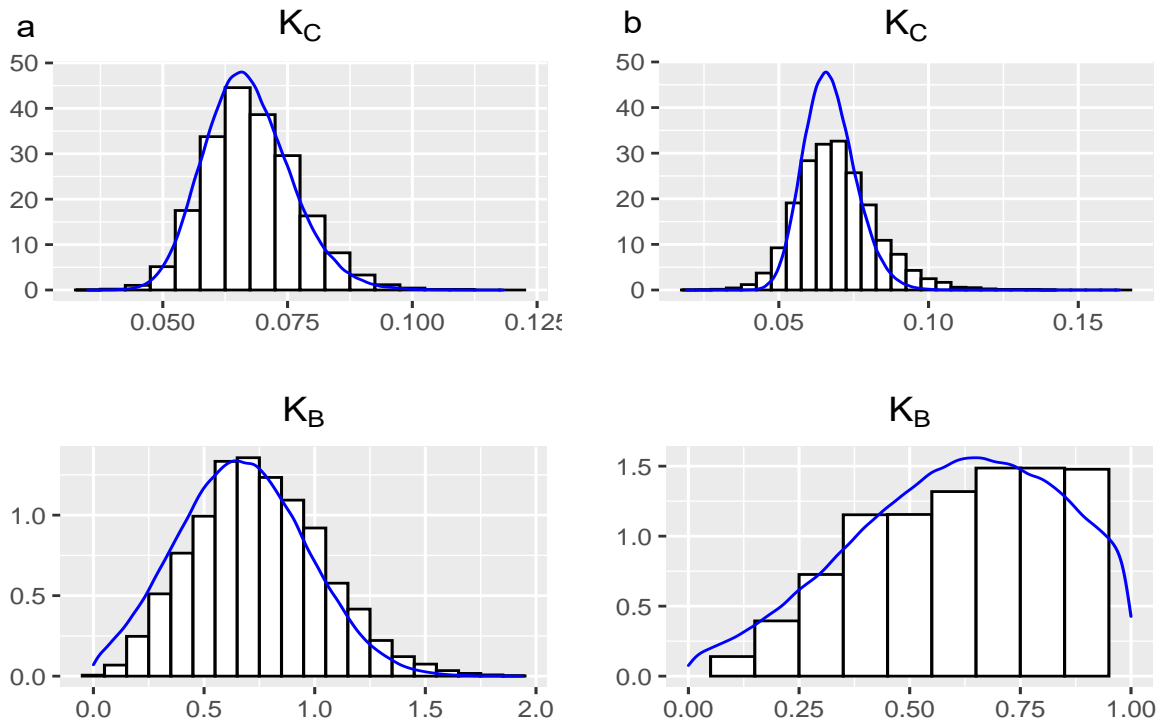


Figure 8: The marginal posterior distributions (histogram) of the SOC and BIO decomposition rates,  $K_C$  and  $K_B$ , respectively, in a) Tarlee and b) Brigalow. The histograms correspond to the three-pool BIO-K model in both Brigalow and Tarlee. The blue densities are the prior distributions of the SOC and BIO decomposition rates.

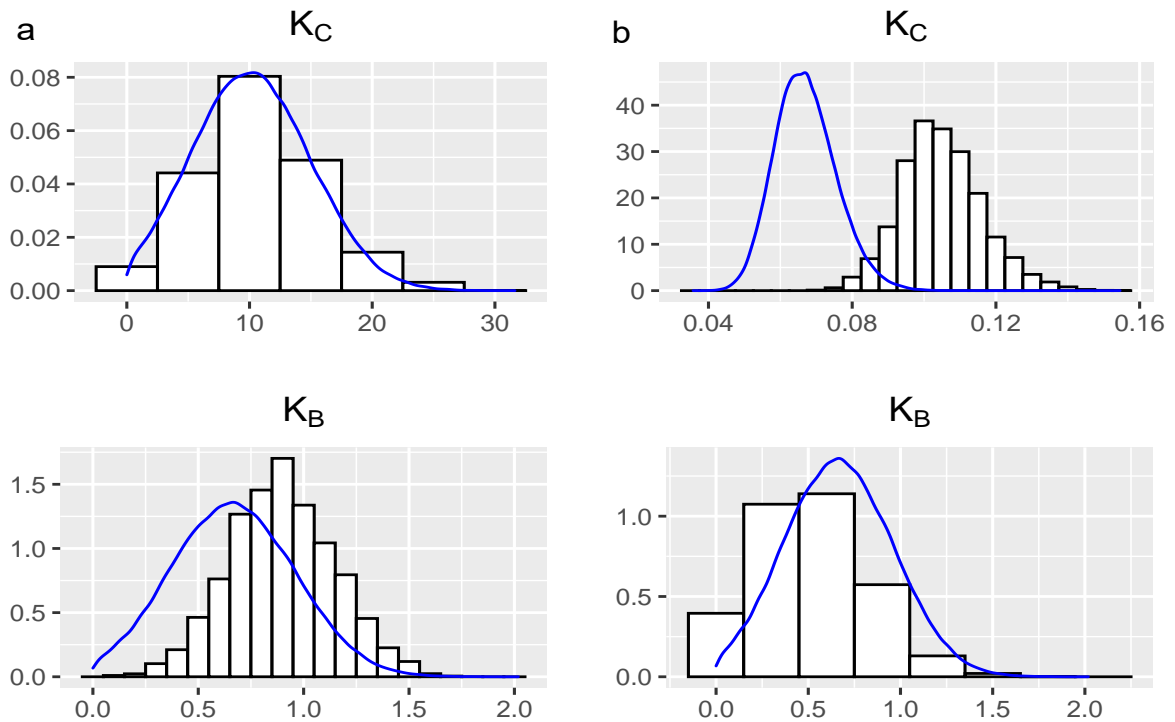


Figure 9: The marginal posterior distributions (histogram) of the SOC and BIO decomposition rates,  $K_C$  and  $K_B$ , respectively, in Broadbalk dataset. The histograms correspond to the three-pool a) BIO-K and b) regular models in Broadbalk. The blue densities are the prior distributions of the SOC and BIO decomposition rates.

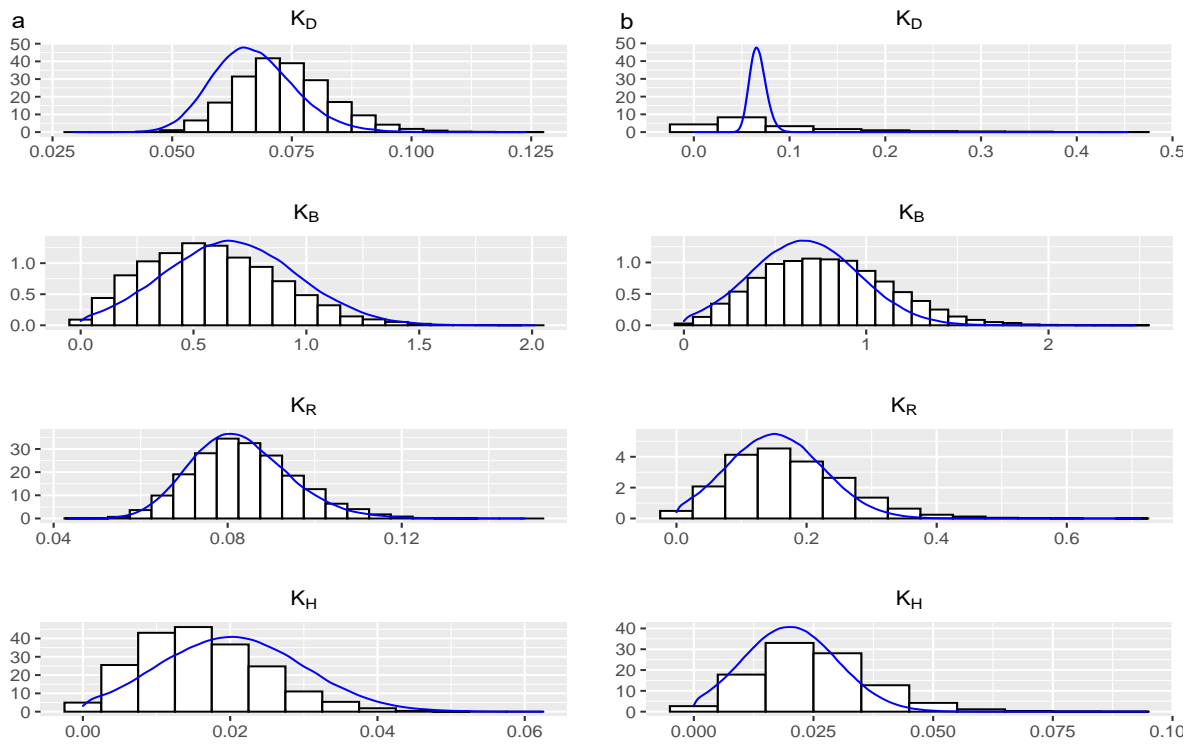


Figure 10: The marginal posterior distributions (histogram) of the decomposition rates of the five-pool BIO-K model in a) Tarlee and b) Brigalow. The blue densities are the prior distributions of the decomposition rates in the five-pool BIO-K model.

## References

- Allenby, G. M. and Rossi, P. E. (2006). Hierarchical Bayes models. *The Handbook of Marketing Research: Uses, Misuses, and Future Advances*, pages 418–440.
- Andrieu, C., Doucet, A., and Holenstein, R. (2010). Particle Markov chain Monte Carlo methods. *Journal of the Royal Statistical Society: Series B (Statistical Methodology)*, 72(3):269–342.
- Auger-Méthé, M., Newman, K., Cole, D., Empacher, F., Gryba, R., King, A. A., Leos-Barajas, V., Flemming, J., Nielsen, A., Petris, G., et al. (2020). An introduction to state-space modeling of ecological time series. *arXiv preprint arXiv:2002.02001*, pages 1–61.
- Berliner, L. M. (1996). Hierarchical Bayesian time series models. In *Maximum entropy and Bayesian methods*, pages 15–22. Springer.
- Blagodatsky, S., Blagodatskaya, E., Yuyukina, T., and Kuzyakov, Y. (2010). Model of apparent and real priming effects: linking microbial activity with soil organic matter decomposition. *Soil Biology and Biochemistry*, 42(8):1275–1283.
- Brooks, S. P. and Gelman, A. (1998). General methods for monitoring convergence of iterative simulations. *Journal of Computational and Graphical Statistics*, 7(4):434–455.
- Bürkner, P.-C., Gabry, J., and Vehtari, A. (2020). Approximate leave-future-out cross-validation for Bayesian time series models. *Journal of Statistical Computation and Simulation*, pages 1–25.
- Clifford, D., Pagendam, D., Baldock, J., Cressie, N., Farquharson, R., Farrell, M., Macdonald, L., and Murray, L. (2014). Rethinking soil carbon modelling: a stochastic approach to quantify uncertainties. *Environmetrics*, 25(4):265–278.
- Cressie, N. and Wikle, C. K. (2015). *Statistics for Spatio-Temporal Data*. John Wiley & Sons.
- Davoudabadi, M. J., Pagendam, D., Drovandi, C., Baldock, J., and White, G. (2021a). Advanced bayesian approaches for state-space models with a case study on soil carbon sequestration. *Environmental Modelling & Software*, 136:104919.
- Davoudabadi, M. J., Pagendam, D., Drovandi, C., Baldock, J., and White, G. (2021b). Modelling and predicting soil carbon sequestration: is current model structure fit for purpose? *arXiv preprint arXiv:2105.04789*.

- Deligiannidis, G., Doucet, A., and Pitt, M. K. (2018). The correlated pseudomarginal method. *Journal of the Royal Statistical Society: Series B (Statistical Methodology)*, 80(5):839–870.
- Doucet, A., De Freitas, N., Murphy, K., and Russell, S. (2000). Rao-Blackwellised particle filtering for dynamic Bayesian networks. In *Proceedings of the Sixteenth conference on Uncertainty in Artificial Intelligence*, pages 176–183. Morgan Kaufmann Publishers Inc.
- Fearnhead, P. and Künsch, H. R. (2018). Particle filters and data assimilation. *Annual Review of Statistics and Its Application*, 5:421–449.
- Fierer, N., Strickland, M. S., Liptzin, D., Bradford, M. A., and Cleveland, C. C. (2009). Global patterns in belowground communities. *Ecology Letters*, 12(11):1238–1249.
- Frey, S. D., Lee, J., Melillo, J. M., and Six, J. (2013). The temperature response of soil microbial efficiency and its feedback to climate. *Nature Climate Change*, 3(4):395–398.
- Gelman, A., Hwang, J., and Vehtari, A. (2014). Understanding predictive information criteria for Bayesian models. *Statistics and Computing*, 24(6):997–1016.
- Gelman, A. and Rubin, D. B. (1992). Inference from iterative simulation using multiple sequences. *Statistical Science*, 7(4):457–472.
- Gordon, N. J., Salmond, D. J., and Smith, A. F. (1993). Novel approach to nonlinear/non-gaussian bayesian state estimation. In *IEE proceedings F (radar and signal processing)*, volume 140, pages 107–113. IET.
- Grandy, A. S. and Neff, J. C. (2008). Molecular c dynamics downstream: the biochemical decomposition sequence and its impact on soil organic matter structure and function. *Science of the Total Environment*, 404(2-3):297–307.
- Jenkinson, D. S., Hart, P. B. S., Rayner, J. H., and Parry, L. C. (1987). Modelling the turnover of organic matter in long-term experiments at Rothamsted. *INTECOL Bulletin*, 15:1–8.
- Juston, J., Andrén, O., Kätterer, T., and Jansson, P. (2010). Uncertainty analyses for calibrating a soil carbon balance model to agricultural field trial data in Sweden and Kenya. *Ecological Modelling*, 221(16):1880–1888.
- Kalman, R. E. (1960). A new approach to linear filtering and prediction problems. *Journal of Basic Engineering*, 82(1):35–45.



- la Cecilia, D., Riley, W. J., and Maggi, F. (2019). Biochemical modeling of microbial memory effects and catabolite repression on soil organic carbon compounds. *Soil Biology and Biochemistry*, 128:1–12.
- Liang, B., Yang, X., He, X., and Zhou, J. (2011). Effects of 17-year fertilization on soil microbial biomass c and n and soluble organic c and n in loessial soil during maize growth. *Biology and Fertility of Soils*, 47(2):121–128.
- Liu, K., Xu, Y., Feng, W., Zhang, X., Yao, S., and Zhang, B. (2020). Modeling the dynamics of protected and primed organic carbon in soil and aggregates under constant soil moisture following litter incorporation. *Soil Biology and Biochemistry*, 151:108039.
- Luo, Y., Ahlström, A., Allison, S. D., Batjes, N. H., Brovkin, V., Carvalhais, N., Chappell, A., Ciais, P., Davidson, E. A., Finzi, A., et al. (2016). Toward more realistic projections of soil carbon dynamics by earth system models. *Global Biogeochemical Cycles*, 30(1):40–56.
- Luo, Z., Wang, E., and Sun, O. J. (2010). Soil carbon change and its responses to agricultural practices in Australian agro-ecosystems: a review and synthesis. *Geoderma*, 155(3):211–223.
- Moorhead, D. L. and Sinsabaugh, R. L. (2006). A theoretical model of litter decay and microbial interaction. *Ecological Monographs*, 76(2):151–174.
- Parton, W. J., Stewart, J. W., and Cole, C. V. (1988). Dynamics of C, N, P and S in grassland soils: a model. *Biogeochemistry*, 5(1):109–131.
- Paul, E. and Clark, F. (1996). Soil microbiology and biochemistry academic press. *New York, USA*.
- Paul, K. I., Polglase, P. J., and Richards, G. P. (2003). Sensitivity analysis of predicted change in soil carbon following afforestation. *Ecological Modelling*, 164(2-3):137–152.
- Riley, W., Maggi, F., Kleber, M., Torn, M., Tang, J., Dwivedi, D., and Guerry, N. (2014). Long residence times of rapidly decomposable soil organic matter: application of a multi-phase, multi-component, and vertically resolved model (bams1) to soil carbon dynamics. *Geoscientific Model Development*, 7(4):1335–1355.
- Rothamsted, E. S. et al. (1978). Details of the classical and long-term experiments 1968-73. *Details of the Classical and Long-Term Experiments 1968-73*.

- Skjemstad, J. and Spouncer, L. (2003). NCAS calibration and verification data. v1. *CSIRO. Data Collection*.
- Skjemstad, J., Spouncer, L., Cowie, B., and Swift, R. (2004). Calibration of the Rothamsted organic carbon turnover model (RothC ver. 26.3), using measurable soil organic carbon pools. *Soil Research*, 42(1):79–88.
- Stamati, F. E., Nikolaidis, N. P., and Schnoor, J. L. (2013). Modeling topsoil carbon sequestration in two contrasting crop production to set-aside conversions with RothC–calibration issues and uncertainty analysis. *Agriculture, Ecosystems & Environment*, 165:190–200.
- Watanabe, S. and Opper, M. (2010). Asymptotic equivalence of Bayes cross validation and widely applicable information criterion in singular learning theory. *Journal of Machine Learning Research*, 11(12).
- Wieder, W. R., Hartman, M. D., Sulman, B. N., Wang, Y.-P., Koven, C. D., and Bonan, G. B. (2018). Carbon cycle confidence and uncertainty: Exploring variation among soil biogeochemical models. *Global Change Biology*, 24(4):1563–1579.
- Woolf, D. and Lehmann, J. (2019). Microbial models with minimal mineral protection can explain long-term soil organic carbon persistence. *Scientific Reports*, 9(1):1–8.
- Xie, H. W., Romero-Olivares, A. L., Guindani, M., and Allison, S. D. (2020). A Bayesian approach to evaluation of soil biogeochemical models. *Biogeosciences*, 17(15):4043–4057.
- Yeluripati, J. B., Van Oijen, M., Wattenbach, M., Neftel, A., Ammann, A., Parton, W., and Smith, P. (2009). Bayesian calibration as a tool for initialising the carbon pools of dynamic soil models. *Soil Biology and Biochemistry*, 41(12):2579–2583.

## Supplementary Material

### A Notation

The notations related to latent variables  $\mathbf{X}$  at time  $t$ , their corresponding measured values  $\mathbf{Y}$  and some model parameters are presented in Table 5. For the sake of notational simplicity we use  $i$

to show fields  $\{1, 2, 3\}$  in the Tarlee dataset, soil type  $\{1, 2, 3\}$  in the Brigalow dataset, and plots  $\{2b, 3, 5, 7, 10, 14\}$  in the Broadbalk dataset. In what follows, we simply use field for all field, soil type and plot.

Notation	Description
$X_{C(t)}^i$	The mass of SOC (t/ha)
$X_{W(t)}^i$	The mass of total wheat dry matter (t/ha)
$X_{S(t)}^i$	The mass of total sorghum dry matter (t/ha)
$X_{Str(t)}^i$	The mass of total straw dry matter (t/ha)
$X_{GW(t)}^i$	The mass of total grain dry matter produced from wheat (t/ha)
$X_{GS(t)}^i$	The mass of total grain dry matter produced from sorghum (t/ha)
$X_G^i(t)$	The mass of total grain dry matter (t/ha)
$X_P^i(t)$	The mass of total pasture dry matter (t/ha)
$X_{IOM(t)}^i$	The mass of IOM (t/ha)
$X_B^i(t)$	The mass of BIO (t/ha)
$X_D^i(t)$	The mass of DPM (t/ha)
$X_R^i(t)$	The mass of resistant plant material (RPM) (t/ha)
$X_H^i(t)$	The mass of HUM (t/ha)
$Y_{TOC(t)}^i$	The measured value of total SOC (TOC) (t/ha)
$Y_{W(t)}^i$	The measured value of total wheat dry matter (t/ha)
$Y_{S(t)}^i$	The measured value of total sorghum dry matter (t/ha)
$Y_{Str(t)}^i$	The measured value of total straw dry matter (t/ha)
$Y_{GW(t)}^i$	The measured value of total wheat grain dry matter (t/ha)
$Y_{GS(t)}^i$	The measured value of total sorghum grain dry matter (t/ha)
$Y_G^i(t)$	The measured value of total grain dry matter (t/ha)
$Y_P^i(t)$	The measured value of total pasture dry matter (t/ha)
$Y_{IOM(t)}^i$	The measured value of IOM (t/ha)
$Y_H^i(t)$	The measured value of HUM (t/ha)
$Y_{POC(t)}^i$	The measured value of particulate organic carbon (POC) (t/ha)
$K_C$	The decay rate of total SOC ( $Y^{-1}$ )
$K_A$	The decay rate of the carbon in pool $A$ ( $Y^{-1}$ )
$\pi_{AB}$	Proportion of the mass of carbon transfer from carbon pool $A$ to carbon pool $B$
$\Delta t$	The yearly time step
$P_D$	Proportion of the carbon input that added to the DPM pool

Table 5: The notations of latent variables, their corresponding measured values and some model parameters.

All processes and all observations, for instance in Tarlee dataset, at time  $t$  in all fields are denoted by  $X_{(t)} = (X_{(t)}^1, X_{(t)}^2, X_{(t)}^3)$  and  $Y_{(t)} = (Y_{(t)}^1, Y_{(t)}^2, Y_{(t)}^3)$ , respectively. All processes at all fields and all times are represented by  $\mathbf{X}$ , and  $\mathbf{Y}$  represents all available data. We denote a set of variables as  $Y_{1:t} = (Y_{(1)}, \dots, Y_{(t)})$ . The log-normal distribution is denoted by  $LN(\mu_1, \sigma_1^2)$  with mean parameter  $\mu_1$  and variance parameter  $\sigma_1^2$  for a log transformation of the random variable.

$N(\mu_2, \sigma_2^2)$  represents the normal distribution with mean and variance  $\mu_2$  and  $\sigma_2^2$ , respectively. Some other notations are presented wherever they are required.

## B Datasets

Tables 6, 7, and 8 show the duration of management treatments in Tarlee, Brigalow, and Broadbalk, respectively.

Management treatments	Field 1	Field 2	Field 3
Wheat for grain	(1979 - 1987) and (1990 - 1996)	-	-
Wheat for hay	1988 and 1989	1989	-
Fallow	1997	1997	1997
Wheat for grain and fallow	-	(1979 - 1988) and (1990 - 1996)	-
Wheat and pasture	-	-	(1979 - 1987)
Wheat and pasture for hay	-	-	1988 and 1989
Wheat for grain and pasture	-	-	(1990 - 1996)

Table 6: The duration of management treatments in three fields in Tarlee.

Management treatments	Soil type 1	Soil type 2	Soil type 3
Cleared	1982	1982	1982
Wheat for grain	(1985 - 1992) and (1994, 1996, 1998)	(1985 - 1992) (1994, 1996, 1998)	(1985 - 1992) (1994, 1996, 1998)
Sorghum for grain	1984, 1995, 1997 and 1999	1984, 1995, 1997 and 1999	1984, 1995, 1997 and 1999
Fallow	1983 and 1993	1983 and 1993	1983 and 1993

Table 7: The duration of management treatments in Brigalow.

## C Prior and Proposal Distributions

The model parameters and their prior probability density functions related to the Tarlee, Brigalow, and Broadbalk datasets are listed in Tables 9, 10, and 11 (to avoid repetition, the priors of the model parameters which have the same distribution in all datasets are presented in Table 9).

Plot	Treatment
2.2 (2b)	35 Mg $ha^{-1}$ fresh farmyard manure every year since 1843.
3	No fertilizer or organic amendments.
5	Mineral fertilizer: 35 kg P $ha^{-1}$ 90 kg K $ha^{-1}$ Na, and Mg. No organic amendments, except that straw was chopped and returned to the plots for 11 years (1869-1879).
7	N2 PKNaMg (until 1967), N2 PK(Na)Mg (from 1968), N2 PKMg (from 1985), and N2 (P)KMg (from 2001)
10	N2, and N4 (from 2001)
14	N2 P $Mg^*$ (until 1967), N2 PK $Mg^*$ (from 1968), N2 $PKMg^*$ (from 1985), and N4 $PK^*(Mg^*)$ (from 2001)

Table 8: The plots and treatments in Broadbalk.

## D Methods

### D.1 Kalman Filter

As the model is a combination of linear and non-linear sub-models, we use the Kalman filter algorithm (Algorithm 1) to draw samples from the posterior and compute the log-likelihood of the linear sub-models. This method is an optimal estimator in the sense of minimising the variance of the estimated state in the case of linear-Gaussian state-space model which has the following form:

$$X_{(t)} = \mathbf{A}^* X_{(t-1)} + \mathbf{B}^* u_{(t)} + \epsilon_{(t)}^*$$

$$Y_{(t)} = \mathbf{C}^* X_{(t)} + \nu_{(t)}^*;$$

where  $\epsilon_{(t)}^* \sim N(\mathbf{0}, \mathbf{Q}^*)$ ,  $\nu_{(t)}^* \sim N(\mathbf{0}, \mathbf{R}^*)$ ,  $\mathbf{A}^*$  is the state-transition matrix, the control-input matrix  $\mathbf{B}^*$  is applied to a known vector of inputs  $u_{(t)}$ , and  $\mathbf{C}^*$  is the observation matrix. Here, the multi-variate normal density with mean vector  $\boldsymbol{\mu}$  and covariance matrix  $\boldsymbol{\Sigma}$  is shown by  $MVN(\boldsymbol{\mu}, \boldsymbol{\Sigma})$ . In Algorithm 1, the Kalman gain matrix is denoted by  $\mathbf{K}_{(t)}$ , and  $X_{(t)}^{t-1}$  and  $\mathbf{P}_{(t)}^{t-1}$  are the expectations of state variable and the process noise, respectively given all observations up to and including time  $t - 1$ .

### D.2 Bootstrap Particle Filter

We draw samples from the posterior of latent variables and estimate the log-likelihood of the non-linear sub-models through the bootstrap particle filter. The algorithm of the bootstrap particle filter is shown in Algorithm 2.

---

**Algorithm 1** Kalman filter algorithm

---

- 1: Initialize with initial state  $\hat{X}_{(0)} = x_{(0)}$  and  $\hat{P}_{(0)} = Q^*$  at  $t = 0$ ;
  - 2: **for**  $t = 1, \dots, T$  **do**
  - 3:      $X_{(t)}^{t-1} = A^* \hat{X}_{(t-1)} + B^* u_{(t)}$ ,     State estimate extrapolation;
  - 4:      $P_{(t)}^{t-1} = A^* \hat{P}_{(t-1)} A^{*'} + Q^*$ ,     State covariance extrapolation;
  - 5:      $K_{(t)} = P_{(t)}^{t-1} C^{*'} [R^* + C^* P_{(t)}^{t-1} C^{*'}]^{-1}$ ,     Kalman gain matrix;
  - 6:      $\hat{X}_{(t)} = X_{(t)}^{t-1} + K_{(t)} [Y_{(t)} - C^* X_{(t)}^{t-1}]$ ,     State estimate update;
  - 7:      $\hat{P}_{(t)} = [I - K_{(t)} C^*] P_{(t)}^{t-1}$ ,     State covariance update;
  - 8:     Compute the log-likelihood contribution,  $l_{(t)}^{\text{KF}}$ , at time  $t$  through the density  $\text{MVN}(Y_{(t)} - C^* X_{(t)}^{t-1}, R^* + C^* P_{(t)}^{t-1} C^{*'})$ ;
  - 9: The complete log-likelihood can be calculated as  $L^* = \sum_t l_{(t)}^{\text{KF}}$
- 

---

**Algorithm 2** Bootstrap particle filter algorithm

---

- 1: **for**  $k = 1, \dots, N$  **do**
  - 2:      $t = 1$ , draw sample  $X_{(1)}^k \sim p(X_{(1)})$ ;
  - 3: **for**  $t = 2, \dots, T$  **do**
  - 4:     **for**  $k = 1, \dots, N$  **do**
  - 5:         Draw sample  $X_{(t)}^k \sim p(X_{(t)} | X_{(t-1)}^{*k})$ ;
  - 6:         Calculate weights  $w_{(t)}^k = p(Y_{(t)} | X_{(t)}^k)$ ;
  - 7:     Estimate the log-likelihood component for the  $t^{\text{th}}$  observation,  $\hat{l}_{(t)} = \log \left( \frac{\sum_j w_{(t)}^j}{N} \right)$ ;
  - 8:     Normalise weights  $W_{(t)}^k = \frac{w_{(t)}^k}{\sum_j w_{(t)}^j}$  for  $k \in \{1, 2, \dots, N\}$ ;
  - 9:     Resample with replacement  $N$  particles  $X_{(t)}^k$  based on the normalised importance weights;
  - 10:     Estimate the overall log-likelihood  $L^* = \sum_t \hat{l}_{(t)}$ .
-

Parameter	Prior	Type
$X_{C(1978)}^1$	Truncated-normal( $40, 5^2, lower = 0$ )	Uninformative
$X_{C(1978)}^2$	Truncated-normal( $40, 5^2, lower = 0$ )	Uninformative
$X_{C(1978)}^3$	Truncated-normal( $40, 5^2, lower = 0$ )	Uninformative
$X_{IOM}$	Truncated-normal( $4, 0.5^2, lower = 0$ )	Uninformative
$K_C$	LN( $-2.71, (0.127)^2$ )	Informative
$K_D$	LN( $-2.71, (0.127)^2$ )	Informative
$K_B$	Truncated-normal( $0.66, 0.3^2, lower = 0$ )	Informative
$K_R$	LN( $-2.5, (0.135)^2$ )	Informative
$K_H$	Truncated-normal( $0.02, 0.01^2, lower = 0$ )	Informative
$c$	N( $0.45, (0.01)^2$ )	Informative
$r_W$	N( $0.5, (0.067)^2$ )	Informative
$r_P$	N( $1, (0.125)^2$ )	Informative
$p$	Beta( $89.9, 809.1$ )	Informative
$h_W$	LN( $0.825, (0.36)^2$ )	Weakly Informative
$\mu_{G_W}$	N( $0.42, (1.18)^2$ )	Weakly Informative
$\mu_P$	N( $1.41, (1.81)^2$ )	Weakly Informative
$\rho_{G_W}$	Uniform( $-1, 1$ )	Uninformative
$\rho_P$	Uniform( $-1, 1$ )	Uninformative
$\sigma_\eta^2$	Truncated-normal( $0, 0.5^2, lower = 0$ )	Uninformative
$\sigma_{\eta_C}^2$	Truncated-normal( $0, 0.5^2, lower = 0$ )	Uninformative
$\sigma_{\eta_D}^2$	Truncated-normal( $0, 0.5^2, lower = 0$ )	Uninformative
$\sigma_{\eta_B}^2$	Truncated-normal( $0, 0.5^2, lower = 0$ )	Uninformative
$\sigma_{\eta_R}^2$	Truncated-normal( $0, 0.5^2, lower = 0$ )	Uninformative
$\sigma_{\eta_H}^2$	Truncated-normal( $0, 0.5^2, lower = 0$ )	Uninformative
$\sigma_{G_W}^2$	Truncated-normal( $0, 0.5^2, lower = 0$ )	Uninformative
$\sigma_W^2$	Truncated-normal( $0, 0.5^2, lower = 0$ )	Uninformative
$\sigma_P^2$	Truncated-normal( $0, 0.5^2, lower = 0$ )	Uninformative
$\pi_{DH}$	Uniform( $0, 1$ )	Uninformative
$\pi_{RH}$	Uniform( $0, 1$ )	Uninformative
$\pi_{HH}$	Uniform( $0, 1$ )	Uninformative
$\pi_{BH}$	Uniform( $0, 1$ )	Uninformative
$\pi_{DB}$	Uniform( $0, 1$ )	Uninformative
$\pi_{RB}$	Uniform( $0, 1$ )	Uninformative
$\pi_{HB}$	Uniform( $0, 1$ )	Uninformative
$\pi_{BB}$	Uniform( $0, 1$ )	Uninformative
$\pi_{CB}$	Uniform( $0, 1$ )	Uninformative
$\pi_{BC}$	Uniform( $0, 1$ )	Uninformative
$P_D$	Uniform( $0, 1$ )	Uninformative
$\sigma_{\epsilon_{TOC}}^2$	0.025	Fixed
$\sigma_{\epsilon_{POC}}^2$	0.9	Fixed
$\sigma_{\epsilon_{G_W}}^2$	0.023	Fixed
$\sigma_{\epsilon_W}^2$	0.133	Fixed
$\sigma_{\epsilon_P}^2$	0.067	Fixed
$\sigma_{\epsilon_{IOM}}^2$	0.01	Fixed
$\sigma_{\epsilon_H}^2$	0.1	Fixed

Table 9: Prior distributions of parameters of the Tarlee dataset and the ones are common in all datasets.

Parameter	Prior	Type
$X_{C(1981)}^1$	Truncated-normal( $60, 5^2, lower = 0$ )	Uninformative
$X_{C(1981)}^2$	Truncated-normal( $60, 5^2, lower = 0$ )	Uninformative
$X_{C(1981)}^3$	Truncated-normal( $60, 5^2, lower = 0$ )	Uninformative
$X_{IOM}$	Truncated-normal( $12, 2^2, lower = 0$ )	Uninformative
$h_S$	LN( $0.46, (1.6)^2$ )	Informative
$\rho_{G_S}$	Uniform( $-1, 1$ )	Uninformative
$\mu_{G_S}$	N( $0.42, (1.18)^2$ )	Weakly Informative
$r_S$	N( $0.5, (0.067)^2$ )	Informative
$K_C$	LN( $-2.71, (0.127)^2$ )	Informative
$K_D$	Truncated-normal( $10, 5^2, lower = 0$ )	Informative
$K_R$	Truncated-normal( $0.15, 0.075^2, lower = 0$ )	Informative
$\sigma_{G_S}^2$	Truncated-normal( $0, 0.5^2, lower = 0$ )	Uninformative
$\sigma_{\eta_B}^2$	Truncated-normal( $0, 0.5^2, lower = 0$ )	Weakly Informative
$\sigma_{\eta_R}^2$	Truncated-normal( $0, 0.5^2, lower = 0$ )	Weakly Informative
$\sigma_{\eta_H}^2$	Truncated-normal( $0, 0.5^2, lower = 0$ )	Weakly Informative
$\sigma_S^2$	Inv-gamma( $0.01, 0.01$ )	Uninformative
$\sigma_{\epsilon_{G_S}}^2$	0.023	Fixed
$\sigma_{\epsilon_S}^2$	0.133	Fixed

Table 10: Prior distributions of parameters of the Brigalow dataset.

Parameter	Prior	Type
$X_{IOM}$	Truncated-normal( $17, 2^2, lower = 0$ )	Uninformative
$\rho_G$	Uniform( $-1, 1$ )	Uninformative
$\rho_{Str}$	Uniform( $-1, 1$ )	Uninformative
$\mu_G$	N( $0.42, (1.18)^2$ )	Weakly Informative
$\mu_{Str}$	N( $0.42, (1.18)^2$ )	Weakly Informative
$K_C$	LN( $-2.71, (0.127)^2$ )	Informative
$K_D$	Truncated-normal( $10, 5^2, lower = 0$ )	Informative
$K_R$	Truncated-normal( $0.15, 0.075^2, lower = 0$ )	Informative
$\sigma_G^2$	Truncated-normal( $0, 0.5^2, lower = 0$ )	Uninformative
$\sigma_{Str}^2$	Truncated-normal( $0, 0.5^2, lower = 0$ )	Weakly Informative
$\sigma_{\epsilon_G}^2$	0.023	Fixed
$\sigma_{\epsilon_{Str}}^2$	0.067	Fixed
$\sigma_{\epsilon_H}^2$	0.1	Fixed
$\sigma_{\epsilon_{POC}}^2$	0.9	Fixed
$X_{C(1852)}^{each\ plot}$	28.8	Fixed

Table 11: Prior distributions of parameters of the Broadbalk dataset.

### D.3 Correlated Pseudo-marginal Method

The process and observation models in our case depend on a set of unknown static parameters  $\theta$ , we treat the parameters as random variables and utilise Bayesian approach to estimate  $\theta$ . Since the posterior distribution and the likelihood are intractable in this study, we utilise correlated



pseudo-marginal method, one of the MCMC methods, to generate a sequence of correlated random samples from a probability distribution. In order to reduce the variance of the ratio of the likelihood estimators  $\hat{p}(\mathbf{Y}|\mathbf{X}, \boldsymbol{\theta}^*)$  and  $\hat{p}(\mathbf{Y}|\mathbf{X}, \boldsymbol{\theta}_{m-1})$  in the acceptance ratio of the CPM method, one can correlate them through correlating the auxiliary random numbers  $U$ , used to obtain these estimators. Algorithms 3 and 4 show the CPM algorithm and the particle filter with a given set of random numbers, respectively.

---

**Algorithm 3** Correlated pseudo-marginal algorithm

---

- 1: Initialise  $\boldsymbol{\theta}_0$ ;
- 2: **for**  $m = 1, \dots, M^*$  **do**
- 3:   Sample  $\boldsymbol{\theta}^* \sim Q(\cdot|\boldsymbol{\theta}_{m-1})$ ;
- 4:   Sample  $\xi \sim N(\mathbf{0}, \mathbf{I})$  and set  $U^* = \tau U_{m-1} + \sqrt{1 - \tau^2} \xi$ ;
- 5:   Compute the estimator  $\hat{p}(\mathbf{Y}|\boldsymbol{\theta}^*, U^*)$  using Algorithm 4
- 6:   Compute the acceptance ratio:

$$r = \frac{\hat{p}(\mathbf{Y}|\boldsymbol{\theta}^*, U^*)p(\boldsymbol{\theta}^*)Q(\boldsymbol{\theta}_{m-1}|\boldsymbol{\theta}^*)}{\hat{p}(\mathbf{Y}|\boldsymbol{\theta}_{m-1}, U_{m-1})p(\boldsymbol{\theta}_{m-1})Q(\boldsymbol{\theta}^*|\boldsymbol{\theta}_{m-1})};$$

- 7:   Accept  $(\boldsymbol{\theta}^*, U^*)$  with probability  $\min(r, 1)$  otherwise, output  $(\boldsymbol{\theta}_{m-1}, U_{m-1})$
- 

---

**Algorithm 4** Particle filter with fixed random numbers

---

- 1: Sample  $U_{(j^*)} \sim N(0, 1)$  and  $V_{(i^*)} \sim N(0, 1)$  for all  $j^* \in \{1, \dots, TN\}$  and  $i^* \in \{1, \dots, T\}$ ;
  - 2: Sample  $X_{(1)}^k \sim p(\cdot|U_{1:N}, \boldsymbol{\theta})$  for all  $k \in \{1, \dots, N\}$ ;
  - 3: **for**  $t = 1, \dots, T-1$  **do**
  - 4:   Sort the collection  $\{X_{(t)}^1, \dots, X_{(t)}^N\}$ ;
  - 5:   Compute importance weights  $w_{(t)}^k$  and log-likelihoods  $\hat{l}_{(t)} = \log \left( \frac{\sum_k w_{(t)}^k}{N} \right)$  for  $k \in \{1, \dots, N\}$ ;
  - 6:   Sample  $X_{(t)}^k$  based on systematic resampling using random values  $V_{1:T}$  and normalised weights  $W_{(t)}^k$  for  $k \in \{1, \dots, N\}$ ;
  - 7:   Set  $X_{(t+1)}^k$  as a sample from  $p(\cdot|X_{(t)}^k, U_{Nt+1:N(t+1)}, \boldsymbol{\theta})$  for  $k \in \{1, \dots, N\}$ ;
  - 8: Estimate the overall log-likelihood  $L^* = \sum_t \hat{l}_{(t)}$ .
- 

## D.4 Predictive Density Estimation

We can compute predictive density in the presence of a state-space model as follows

$$p(Y_{t+1}|Y_{1:t}) = \int_{\Theta} \int_{\mathcal{X}} p(Y_{t+1}|X_t, \theta, Y_{1:t})p(X_t|\theta, Y_{1:t})p(\theta|Y_{1:t})dX d\theta.$$

As the above integrals typically do not have closed-form solutions, we estimate them based on  $J_1$  MCMC samples and  $J_2$  particles getting from an SMC algorithm

$$p(\hat{Y}_{t+1}|Y_{1:t}) = \frac{1}{J_1} \sum_{j_1=1}^{J_1} \frac{1}{J_2} \sum_{j_2=1}^{J_2} p(Y_{t+1}|X_t^{j_2}, \theta^{j_1}, Y_{1:t}).$$

We can estimate the posterior variance of the log predictive density in practice by

$$\sum_{t=1}^T \left\{ \frac{1}{S-1} \sum_{s=1}^S [\log p(Y_t|\theta^s) - \overline{\log p(Y_t|\theta^*)}]^2 \right\}$$

where  $S = J_1 + J_2$  and  $\theta$  includes the vector of parameters  $\theta$  and state variables.

## E Three-pool Model

### E.1 Process Model

The process model of the three-pool model at time  $t$  in field  $i$  is:

$$\begin{aligned} \log(X_{C(t)}^i) &= \log(X_{C(t-1)}^i e^{-K_C F(t-1)\Delta t} + I_{C(t)}^i) \\ &\quad + \pi_{BC}(U_{(t-1)}^i - \min(U_{(t-1)}^i, \kappa_{BIO} X_{Total(t-1)}^i - X_{B(t-1)}^i)) \\ &\quad + X_{B(t-1)}^i (1 - e^{-K_B F(t-1)\Delta t}) \pi_{BC} + \eta_{C(t)}^i, \quad \eta_{C(t)}^i \sim N(0, \sigma_{\eta_C}^2); \end{aligned} \quad (8)$$

$$\begin{aligned} \log(X_{B(t)}^i) &= \log(X_{B(t-1)}^i e^{-K_B F(t-1)\Delta t} + \min(U_{(t-1)}^i, \kappa_{BIO} X_{Total(t-1)}^i - X_{B(t-1)}^i)) \\ &\quad + \eta_{B(t)}^i, \quad \eta_{B(t)}^i \sim N(0, \sigma_{\eta_B}^2); \end{aligned} \quad (9)$$

$$U_{(t-1)}^i = X_{C(t-1)}^i (1 - e^{-K_C F(t-1)\Delta t}) \pi_{CB} + X_{B(t-1)}^i (1 - e^{-K_B F(t-1)\Delta t}) \pi_{BB}$$

$$X_{G_W(t)}^i \sim LN(\mu_{G_W} + \rho_{G_W}(\log(X_{G_W(t-1)}^i) - \mu_{G_W}), \sigma_{G_W}^2); \quad (10)$$

$$X_{W(t)}^i \sim LN(\log h_W + \log(x_{G_W(t)}^i), \sigma_W^2); \quad (11)$$

$$X_{P(t)}^i \sim LN(\mu_P + \rho_P(\log(X_{P(t-1)}^i) - \mu_P), \sigma_P^2); \quad (12)$$

$$X_{G_S(t)}^i \sim LN(\mu_{G_S} + \rho_{G_S}(\log(X_{G_S(t-1)}^i) - \mu_{G_S}), \sigma_{G_S}^2); \quad \text{and} \quad (13)$$

$$X_{S(t)}^i \sim LN(\log h_S + \log(x_{G_S(t)}^i), \sigma_S^2); \quad (14)$$

$$X_{G(t)}^i \sim LN(\mu_G + \rho_G(\log(X_{G(t-1)}^i) - \mu_G), \sigma_G^2); \quad (15)$$

$$X_{Str(t)}^i \sim LN(\mu_{Str} + \rho_{Str}(\log(X_{Str(t-1)}^i) - \mu_{Str}), \sigma_{Str}^2); \quad (16)$$

$$X_{IOM(t)}^i = M; \quad (17)$$

where  $M$  is an unknown constant value,  $F_{(t-1)} = \frac{X_{B(t-1)}^i}{X_{Total(t-1)}^i \kappa_{BIO}}$ , and  $\kappa_{BIO} = 0.05$ . Also,  $h_W$ ,  $h_S$ ,  $\rho_P$ ,  $\rho_{G_W}$ ,  $\rho_{G_S}$ , and  $\rho_{Str}$  denote the harvest index which is the ratio of wheat to grain, the harvest index which is the ratio of sorghum to grain, auto-regressive parameters for the evolution of pasture total dry matter (TDM) and grain TDM of wheat, sorghum, and straw, respectively. The mass of carbon inputs,  $I_{C(t)}^i$ , for the Tarlee, Brigalow, and Rothamsted datasets is denoted by  $IT_{C(t)}^i$ ,  $IB_{C(t)}^i$  and  $IR_{C(t)}^i$ , respectively which are:

$$IT_{C(t)}^i = \begin{cases} c(X_{W(t)}^i - X_{G_W(t)}^i) + cr_W X_{W(t)}^i & \text{Wheat for Grain} \\ cpX_{W(t)}^i + cr_W X_{W(t)}^i & \text{Wheat for Hay} \\ cX_{P(t)}^i + cr_P X_{P(t)}^i & \text{Pasture} \\ cpX_{P(t)}^i + cr_P X_{P(t)}^i & \text{Pasture for Hay} \\ 0 & \text{Fallow} \end{cases}$$

$$IB_{C(t)}^i = \begin{cases} c(X_{W(t)}^i - X_{G_W(t)}^i) + cr_W X_{W(t)}^i & \text{Wheat for Grain} \\ cpX_{W(t)}^i + cr_W X_{W(t)}^i & \text{Wheat for Hay} \\ c(X_{S(t)}^i - X_{G_S(t)}^i) + cr_S X_{S(t)}^i & \text{Sorghum for Grain} \\ cpX_{S(t)}^i + cr_S X_{S(t)}^i & \text{Sorghum for Hay} \\ 0 & \text{Fallow} \end{cases}$$

and

$$IR_{C(t)}^i = \begin{cases} cX_{Str(t)}^i + cr_W (X_{G(t)}^i + X_{Str(t)}^i) & \text{Wheat for Grain} \\ 0 & \text{Fallow} \end{cases}$$

where  $p$ ,  $r_P$ ,  $r_S$ , and  $r_W$  are the proportion of the crop left above-ground after harvest, the root-to-shoot ratios (in terms of TDM) for pasture, sorghum and wheat crops, respectively. The amount of carbon that enters into the soil from plant-matters that remains above-ground after harvesting

wheat and sorghum for grain are  $c(X_{W(t)}^i - X_{G_W(t)}^i)$ , and  $c(X_{S(t)}^i - X_{G_S(t)}^i)$ , respectively. This amount for straw is considered by  $cX_{Str(t)}^i$  in the Broadbalk dataset. The amount of carbon comes from below-ground for wheat and sorghum are then  $cr_W X_{W(t)}^i$  and  $cr_S X_{S(t)}^i$ , respectively. Here,  $c$  is the carbon content of dry plant matter. The amount of carbon that comes from below and above-ground (i.e., roots and what remains after harvesting) are included in  $IT_{C(t)}^i$ ,  $IB_{C(t)}^i$ , and  $IR_{C(t)}^i$ .

## E.2 Observation Model

This section is allocated to show the observation model of the three-pool model. The observation models of total organic carbon (TOC), IOM, and input carbon are shown in equations (18)-(26). As the measurements (18)-(26) are independent, we can show the joint observation model of them at time  $t$  and field  $i$  by multiplying the probability of each measurement variable given the corresponding latent variable and parameter  $\theta$ . The overall observation model across all  $i$ 's is therefore:

$$p(Y_{(t)}|X_{(t)}, \theta) = \prod_i p(Y_{(t)}^i|X_{(t)}^i, \theta),$$

where  $Y_{(t)}^i = (Y_{TOC(t)}^i, Y_{IOM(t)}^i, Y_{G_W(t)}^i, Y_{G(t)}^i, Y_{W(t)}^i, Y_{P(t)}^i, Y_{G_S(t)}^i, Y_{Str(t)}^i, Y_{S(t)}^i)$  and  $X_{(t)}^i = (X_{C(t)}^i, X_{B(t)}^i, X_{G_W(t)}^i, X_{G(t)}^i, X_{W(t)}^i, X_{P(t)}^i, X_{G_S(t)}^i, X_{Str(t)}^i, X_{S(t)}^i, X_{IOM(t)}^i)$ .

$$\begin{aligned} Y_{TOC(t)}^i|X_{C(t)}^i &= x_{C(t)}^i, X_{IOM(t)}^i = x_{IOM(t)}^i \\ &, X_{B(t)}^i = x_{B(t)}^i \sim LN(\log(x_{C(t)}^i + x_{IOM(t)}^i + x_{B(t)}^i), \sigma_{\epsilon_{TOC}}^2). \end{aligned} \quad (18)$$

$$Y_{IOM(t)}^i|X_{IOM(t)}^i = x_{IOM(t)}^i \sim LN(\log(x_{IOM(t)}^i), \sigma_{\epsilon_{IOM}}^2); \quad (19)$$

$$Y_{G_W(t)}^i|X_{G_W(t)}^i = x_{G_W(t)}^i \sim LN(\log(x_{G_W(t)}^i), \sigma_{\epsilon_{G_W}}^2); \quad (20)$$

$$Y_{W(t)}^i|X_{W(t)}^i = x_{W(t)}^i \sim LN(\log(x_{W(t)}^i), \sigma_{\epsilon_W}^2); \quad (21)$$

$$Y_{P(t)}^i|X_{P(t)}^i = x_{P(t)}^i \sim LN(\log(x_{P(t)}^i), \sigma_{\epsilon_P}^2); \quad (22)$$

$$Y_{G_S(t)}^i|X_{G_S(t)}^i = x_{G_S(t)}^i \sim LN(\log(x_{G_S(t)}^i), \sigma_{\epsilon_{G_S}}^2); \quad (23)$$

$$Y_{S(t)}^i|X_{S(t)}^i = x_{S(t)}^i \sim LN(\log(x_{S(t)}^i), \sigma_{\epsilon_S}^2). \quad (24)$$

$$Y_{G(t)}^i|X_{G(t)}^i = x_{G(t)}^i \sim LN(\log(x_{G(t)}^i), \sigma_{\epsilon_G}^2); \quad \text{and} \quad (25)$$

$$Y_{Str(t)}^i|X_{Str(t)}^i = x_{Str(t)}^i \sim LN(\log(x_{Str(t)}^i), \sigma_{\epsilon_{Str}}^2). \quad (26)$$

## F Five-pool Model

### F.1 Process Model

The process model of the five-pool model is shown by (27)-(30). This model also includes sub-models (10)-(17).

$$\log(X_{D(t)}^i) = \log(X_{D(t-1)}^i e^{-K_D \Delta t} + P_D I_C^i) + \eta_{D(t)}^i, \quad \eta_{D(t)}^i \sim N(0, \sigma_{\eta_D}^2); \quad (27)$$

$$\log(X_{R(t)}^i) = \log(X_{R(t-1)}^i e^{-K_R F(t-1) \Delta t} + (1 - P_D) I_C^i) + \eta_{R(t)}^i, \quad \eta_{R(t)}^i \sim N(0, \sigma_{\eta_R}^2); \quad (28)$$

$$\begin{aligned} \log(X_{H(t)}^i) = & \log(X_{H(t-1)}^i e^{-K_H F(t-1) \Delta t} + X_{D(t-1)}^i (1 - e^{-K_D F(t-1) \Delta t}) \pi_{DH} \\ & + X_{R(t-1)}^i (1 - e^{-K_R F(t-1) \Delta t}) \pi_{RH} + X_{H(t-1)}^i (1 - e^{-K_H F(t-1) \Delta t}) \pi_{HH} \\ & + X_{B(t-1)}^i (1 - e^{-K_B F(t-1) \Delta t}) \pi_{BH}) + \pi_{BH}(U_{(t-1)}^i \\ & - \min(U_{(t-1)}^i, \kappa_{BIO} X_{Total(t-1)}^i - X_{B(t-1)}^i)) + \eta_{H(t)}^i, \quad \eta_{H(t)}^i \sim N(0, \sigma_{\eta_H}^2); \end{aligned} \quad (29)$$

$$\log(X_{B(t)}^i) = \log(X_{B(t-1)}^i e^{-K_B F(t-1) \Delta t} + \min(U_{(t-1)}^i, \kappa_{BIO} X_{Total(t-1)}^i - X_{B(t-1)}^i)) \sim N(0, \sigma_{\eta_B}^2); \quad (30)$$

where

$$\begin{aligned} U_{(t-1)}^i = & X_{D(t-1)}^i (1 - e^{-K_D F(t-1) \Delta t}) \pi_{DB} + X_{R(t-1)}^i (1 - e^{-K_R F(t-1) \Delta t}) \pi_{RB} \\ & + X_{H(t-1)}^i (1 - e^{-K_H F(t-1) \Delta t}) \pi_{HB} + X_{B(t-1)}^i (1 - e^{-K_B F(t-1) \Delta t}) \pi_{BB} \end{aligned} \quad (31)$$

Since the transition densities of the latent variables in this model are independent, the transition density of the joint process model of the latent variables can be gained through multiplying them.

### F.2 Observation Model

The observation models of the IOM pool and carbon input which are presented by equations (19)-(26) are the same in this model. The observation models of the TOC, particulate organic carbon (POC), and HUM are

$$\log(Y_{TOC(t)}^i) = \log(x_{D(t)}^i + x_{IOM(t)}^i + x_{B(t)}^i + x_{R(t)}^i + x_{H(t)}^i) + \eta_{\epsilon TOC}, \quad (32)$$

$$\eta_{\epsilon TOC} \sim N(0, \sigma_{\epsilon TOC}^2);$$

$$\log(Y_{POC(t)}^i) = \log(x_{D(t)}^i + x_{B(t)}^i + x_{R(t)}^i) + \eta_{\epsilon POC}, \quad \eta_{\epsilon POC} \sim N(0, \sigma_{\epsilon POC}^2); \quad (33)$$

$$\log(Y_{H(t)}^i) = \log(x_{H(t)}^i) + \eta_{\epsilon H}, \quad \eta_{\epsilon H} \sim N(0, \sigma_{\epsilon H}^2). \quad (34)$$

Since the measurements are independent, the joint observation model of them at time  $t$  and field  $i$ , and the overall observation model across all  $i$ 's can be gained similar to what we mentioned in the observation model of the three-pool model.

## G Gelman and Rubin's convergence diagnostic statistic

Parameter	$\hat{R}$	Upper C.I. bound on $\hat{R}$
$K_C$	1.00	1.00
$c$	1.00	1.00
$r_W$	1.00	1.00
$r_P$	1.00	1.00
$p$	1.00	1.00
$h_W$	1.00	1.01
$\mu_{G_W}$	1.00	1.01
$\mu_P$	1.00	1.01
$\rho_{G_W}$	1.00	1.01
$\rho_P$	1.00	1.01
$\sigma_{\eta_C}^2$	1.00	1.01
$\sigma_{G_W}^2$	1.00	1.00
$\sigma_W^2$	1.01	1.02
$\sigma_P^2$	1.00	1.00
$X_{IOM}$	1.00	1.00
$X_{C(1978)}^1$	1.00	1.00
$X_{C(1978)}^2$	1.00	1.01
$X_{C(1978)}^3$	1.00	1.00
$\sigma_{\eta_B}^2$	1.01	1.03
$K_B$	1.00	1.00
$\pi_{CB}$	1.01	1.03
$\pi_{BB}$	1.00	1.00
$\pi_{BC}$	1.00	1.00

Table 12: The Gelman and Rubin's convergence diagnostic,  $\hat{R}$  calculated for model parameters of the three-pool model of the Tarlee dataset. Since the point estimate of  $\hat{R}$  for each parameter is less than 1.2, the MCMC samples can be considered to have reached a stationary distribution and are mixing adequately.

Parameter	$\hat{R}$	Upper C.I. bound on $\hat{R}$
$K_C$	1.00	1.00
$c$	1.00	1.00
$r_W$	1.00	1.00
$p$	1.01	1.03
$h_W$	1.00	1.00
$\mu_{G_W}$	1.04	1.13
$\mu_{G_S}$	1.04	1.05
$\rho_{G_W}$	1.00	1.01
$\sigma_{\eta_C}^2$	1.01	1.02
$\sigma_{G_W}^2$	1.00	1.00
$\sigma_W^2$	1.00	1.00
$X_{IOM}$	1.00	1.00
$X_{C(1982)}^1$	1.01	1.02
$X_{C(1982)}^2$	1.01	1.02
$X_{C(1982)}^3$	1.00	1.00
$r_S$	1.00	1.00
$\sigma_{\eta_B}^2$	1.02	1.08
$\sigma_S^2$	1.17	1.34
$K_B$	1.00	1.00
$K_R$	1.00	1.00
$\pi_{DB}$	1.00	1.01
$\pi_{BB}$	1.00	1.02
$\pi_{BC}$	1.00	1.01
$\pi_{CB}$	1.00	1.01
$\mu_{G_S}$	1.00	1.00
$\rho_{G_S}$	1.00	1.00
$\sigma_{G_S}^2$	1.00	1.00
$h_S$	1.01	1.02

Table 13: The Gelman and Rubin's convergence diagnostic,  $\hat{R}$  calculated for model parameters of the three-pool model of the Brigalow dataset. Since the point estimate of  $\hat{R}$  for each parameter is less than 1.2, the MCMC samples can be considered to have reached a stationary distribution and are mixing adequately.



Parameter	$\hat{R}$	Upper C.I. bound on $\hat{R}$
$K_C$	1.01	1.03
$c$	1.00	1.00
$r_W$	1.01	1.02
$\mu_G$	1.03	1.10
$\mu_{Str}$	1.00	1.00
$\rho_G$	1.00	1.01
$\rho_{Str}$	1.00	1.01
$\sigma_{\eta_C}^2$	1.14	1.27
$\sigma_G^2$	1.00	1.00
$\sigma_{Str}^2$	1.00	1.00
$X_{IOM}$	1.00	1.01
$\sigma_{\eta_B}^2$	1.06	1.08
$K_B$	1.00	1.00
$\pi_{BB}$	1.00	1.00
$\pi_{BC}$	1.01	1.03
$\pi_{CB}$	1.00	1.00

Table 14: The Gelman and Rubin's convergence diagnostic,  $\hat{R}$  calculated for model parameters of the three-pool BIO-K model of the Broadbalk dataset. Since the point estimate of  $\hat{R}$  for each parameter is less than 1.2, the MCMC samples can be considered to have reached a stationary distribution and are mixing adequately.

Parameter	$\hat{R}$	Upper C.I. bound on $\hat{R}$
$K_C$	1.00	1.00
$c$	1.00	1.01
$r_W$	1.00	1.01
$\mu_G$	1.00	1.00
$\mu_{Str}$	1.00	1.00
$\rho_G$	1.00	1.00
$\rho_{Str}$	1.00	1.00
$\sigma_{\eta_C}^2$	1.00	1.00
$\sigma_G^2$	1.00	1.00
$\sigma_{Str}^2$	1.00	1.00
$X_{IOM}$	1.00	1.00
$\sigma_{\eta_B}^2$	1.04	1.12
$K_B$	1.02	1.05
$\pi_{BB}$	1.00	1.01
$\pi_{BC}$	1.16	1.46
$\pi_{CB}$	1.02	1.03

Table 15: The Gelman and Rubin's convergence diagnostic,  $\hat{R}$  calculated for model parameters of the three-pool regular model of the Broadbalk dataset. Since the point estimate of  $\hat{R}$  for each parameter is less than 1.2, the MCMC samples can be considered to have reached a stationary distribution and are mixing adequately.